DOE/NASA/0061-79/1
NASA CR-159589
AER 1713

15 kWe (NOMINAL) SOLAR THERMAL ELECTRIC POWER CONVERSION CONCEPT DEFINITION STUDY — STEAM RANKINE TURBINE SYSTEM

Timothy Bland
Sundstrand Corporation

October 1979

Prepared for

National Aeronautics and Space Administration
Lewis Research Center
Under Contract DEN 3-61

for

U.S. DEPARTMENT OF ENGERY
Office of Solar, Geothermal, Electric and Storage Systems
Division of Central Solar Technology

DOE/NASA/0061-79/1
NASA CR-159589
AER1713

15 kWe (NOMINAL) SOLAR THERMAL ELECTRIC POWER CONVERSION CONCEPT DEFINITION STUDY — STEAM RANKINE TURBINE SYSTEM

Timothy Bland
Sundstrand Corporation
Rockford, Illinois 61101

October 1979

Prepared for

National Aeronautics and Space Administration
Lewis Research Center
Cleveland, Ohio 44135
Under Contract DEN 3-61

For

U.S. DEPARTMENT OF ENERGY
Office of Solar, Geothermal, Electric and Storage Systems
Division of Central Solar Technology
Washington, D.C. 20545
Under Interagency Agreement EX-76-A-29-1060

TABLE OF CONTENTS

LIST OF FIGURES

LIST OF TABLES

1.0 SUMMARY

A study was performed to identify a steam Rankine cycle power conversion system which would have an efficiency higher than that achieved by currently available steam systems, at power levels associated with point-focused solar receivers.

The first task of the study was to perform parametric analyses of a single-stage turbine powered system to define optimum performance characteristics for 15 kilowatt, 60 Hz electrical output. A system design optimization computer program was generated modeling the components of the system and was used to generate families of optimum systems for different steam temperatures, where optimum refers to weight and efficiency.

Similar parametric analyses in somewhat less detail were performed for a two-stage re-entry steam turbine system with reheat between stages and a single-stage organic Rankine turbine system using Toluene as the working fluid. At the maximum acceptable turbine inlet temperatures of 732°C (1350°F) for steam and 427°C (800°F) for Toluene, system efficiencies of 23.2% and 27% were obtained for single and two-stage steam respectively and 27.5% for the Toluene system, where system efficiency is defined as 6(Hertz A.C. electrical power output divided by absorbed thermal power input in the working fluid.

A detailed conceptual design was subsequently generated for the two-stage steam turbine system including a system outline drawing produced to delineate overall envelope dimensions. System hydraulic, power flow and control schematics were generated and control techniques developed to satisfy various operating modes. System off-design performance calculations were made to determine total annual power production, and these showed that the efficiency did not decrease drastically even down to 50% of thermal input power. In addition, the system would be self-sustaining down to about 10% of thermal input power.

Cost estimates were made for mass-producing the system and it was found that at very high production rates the system cost would be approximately 364 dollars/kw. Operation and maintenance costs were estimated from component failure rates and scheduled maintenance requirements and were found to be about 0.0078 dollars/kw-hr.

The principal conclusion of the study was that relatively high steam turbine Rankine system efficiencies are achievable with good off-design performance. However, advancement of the state-of-the-art, in the form of turbine interstage sealing techniques, is required to achieve this performance.

2.0 INTRODUCTION

This study arises from the need to define high-efficiency heat engines for operation in combination with point-focused solar collectors for electrical power generation. The study is one of several generated under the 'Solar Thermal Power Systems Point-Focusing Distributed Receiver Technology Program' of the Department of Energy Thermal Power Systems Branch (Reference 1). References 2, 3, 4, 5, and 6 are the reports on the other related power conversion systems.

The requirements of the study contract were to investigate performance potential and provide a conceptual design of a single-stage steam turbine engine. Potential efficiency improvements associated with the utilization of a two-stage system with reheat were to be investigated as a lower-level task. However, preliminary performance calculations led to the decision by NASA to redirect the program to require the system design to be performed on the two-stage system. Based on a NASA inquiry, preliminary performance estimates were made of an organic Rankine cycle engine using Toluene as the working fluid to provide performance comparisons of the different fluids.

The procedure for selecting the design point was to generate optimized designs using a multi-variable optimization technique in conjunction with the computer program used to model the system. Selection of maximum system temperature was based on current metallurgical data.

The conceptual design was performed to meet the design point operating requirements, to enable the system to interface adequately with a heat receiver design and to be capable of matching all anticipated operating modes. The resulting design was drafted in sufficient detail to allow a manufacturing assessment to be performed.

The author wishes to express his appreciation to Larry Ludwig and Al Kascak of the NASA LeRc Seals and Rotor Dynamics Group for their assistance in the preliminary design of the gas thrust bearing necessary for satisfactory operation of the system.

3.0 PARAMETRIC ANALYSIS

3.1 ANALYTICAL TECHNIQUES

A system design computer program was modified to model the system components and their interactions. The design concept utilized a closed hermetic, regenerative, steam Rankine system consisting of a combined rotating unit (CRU) comprising the turbine, alternator, and pump all on a common shaft and supported by working-fluid lubricated, hydrodynamic bearings; a regenerator to recover turbine exhaust superheat for feedwater preheating; a forced-air-cooled condenser; and a hot well with boost pump to provide bearing lubricant flow and system flow to the feed pump. The preliminary concept is shown in Figure 1 and the final concept shown in Figure 2.

Subroutines were used to design and determine the performance of major system components. These included the turbine, boiler feed pump, bearings, feedwater heater and condenser. The turbine type employed was a supersonic, axial flow impulse design where output power and efficiency as a function of mass flow rate were used for the solution of a system design point. The feedwater pump performance was correlated with specific speed data for the pitot pump configuration selected. Bearing design information was based on operating speeds, calculated rotor weights and selected requirements of minimum film thickness.

The feedwater heater, or regenerator, design was based on friction factor and Colburn 'j' factor information from Reference 7 for the selected heat exchanger configuration, which was a finned tube type. The overall size and pressure drops were a function of the heat load. The performance was based on heat exchanger effectiveness relationships as a function of number of heat transfer units (NTU) for a counterflow heat exchanger.

A similar technique was used for the condenser design using effectiveness - NTU relationships appropriate to a crossflow heat exchanger with condensation. Again, a finned tube configuration was selected from Reference 7.

A homopolar inductor alternator was selected and modeled using available data. Condenser fan and fan motor performance was based on commercially available fan designs.

The system design program employed detailed component design subroutines which allowed system performance and weight to be calculated for a given set of input parameters. The basic program flow chart is presented in Figure 3. The program iterated the system flow and flow dependent component efficiencies to determine the mass flow required for the net electrical output power specified.

System state points were then determined, allowing system efficiency to be calculated based upon useful 60 Hz electrical power out and heat absorbed in the heat receiver.

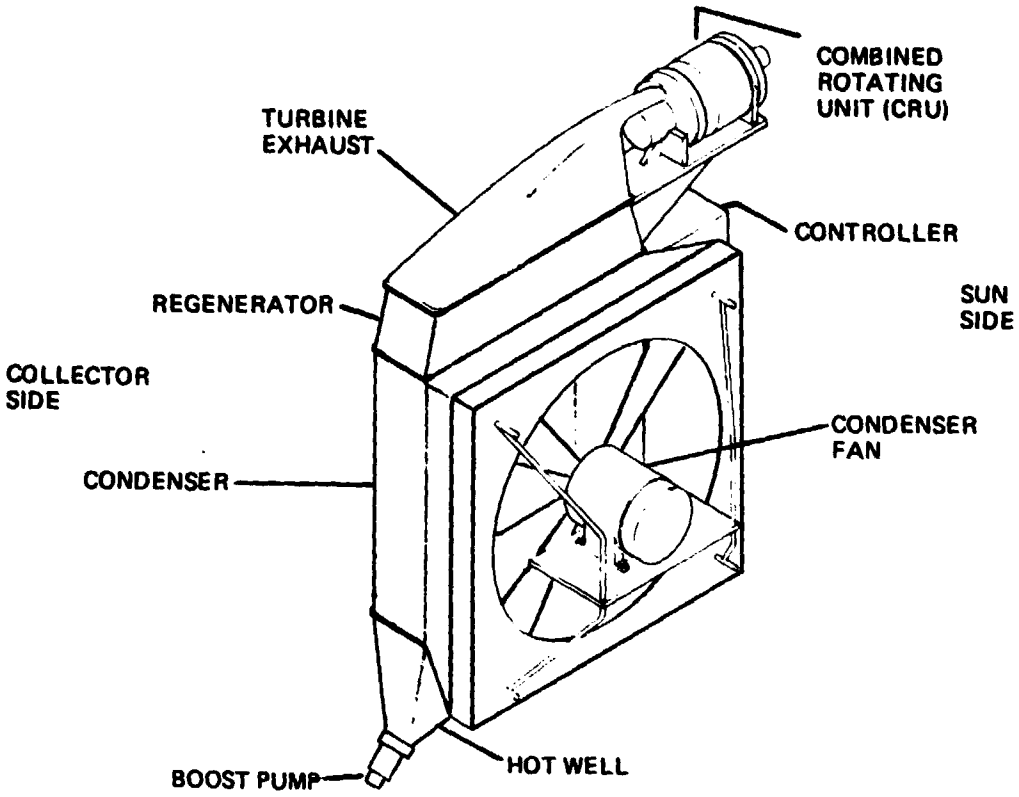

Figure 1 15 KW_e Preliminary System

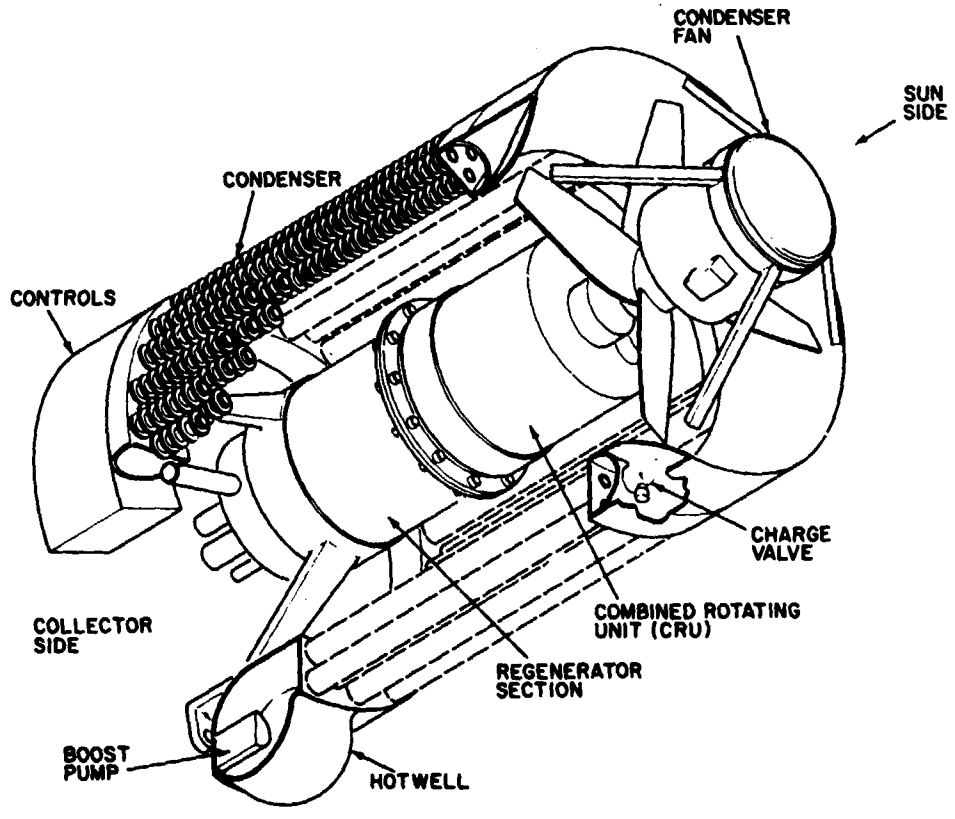

Figure 2 Final Concept

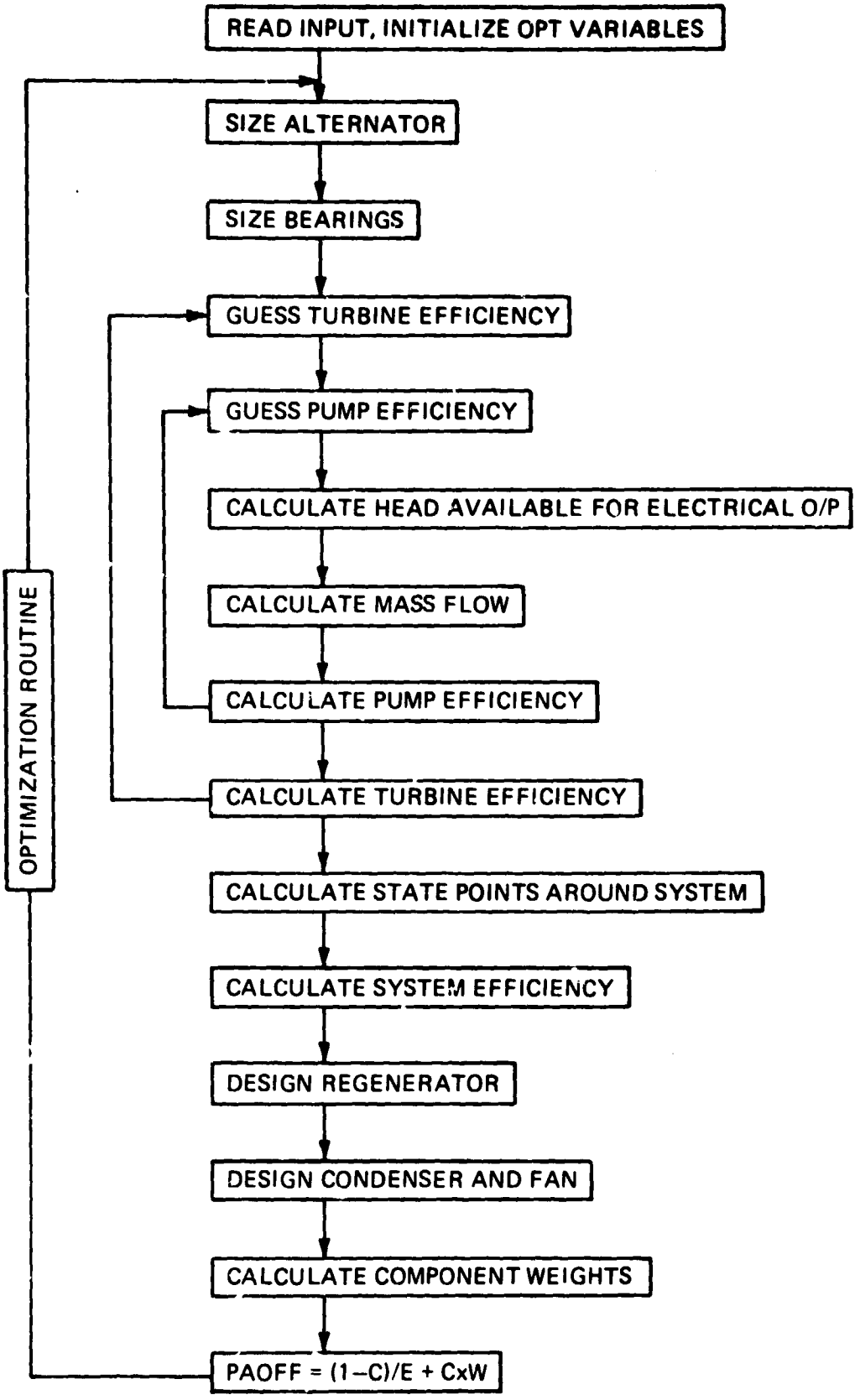

Figure 3 Design Program Flow Chart

A system optimization subroutine was incorporated which was used to generate a family of designs representing systems varying from maximum efficiency to minimum weight. This routine operates by seeking to minimize a function, PAOFF, defined by

$$PAOFF = \frac{1-C}{E} + C(W)$$

where C = Weighting factor

E = System efficiency

W = System weight

It can be seen that if C = O, the optimization routine will seek to maximize efficiency with no consideration for weight, while if C = 1, the weight will be minimized with no consideration for efficiency. This is shown in Figure 4.

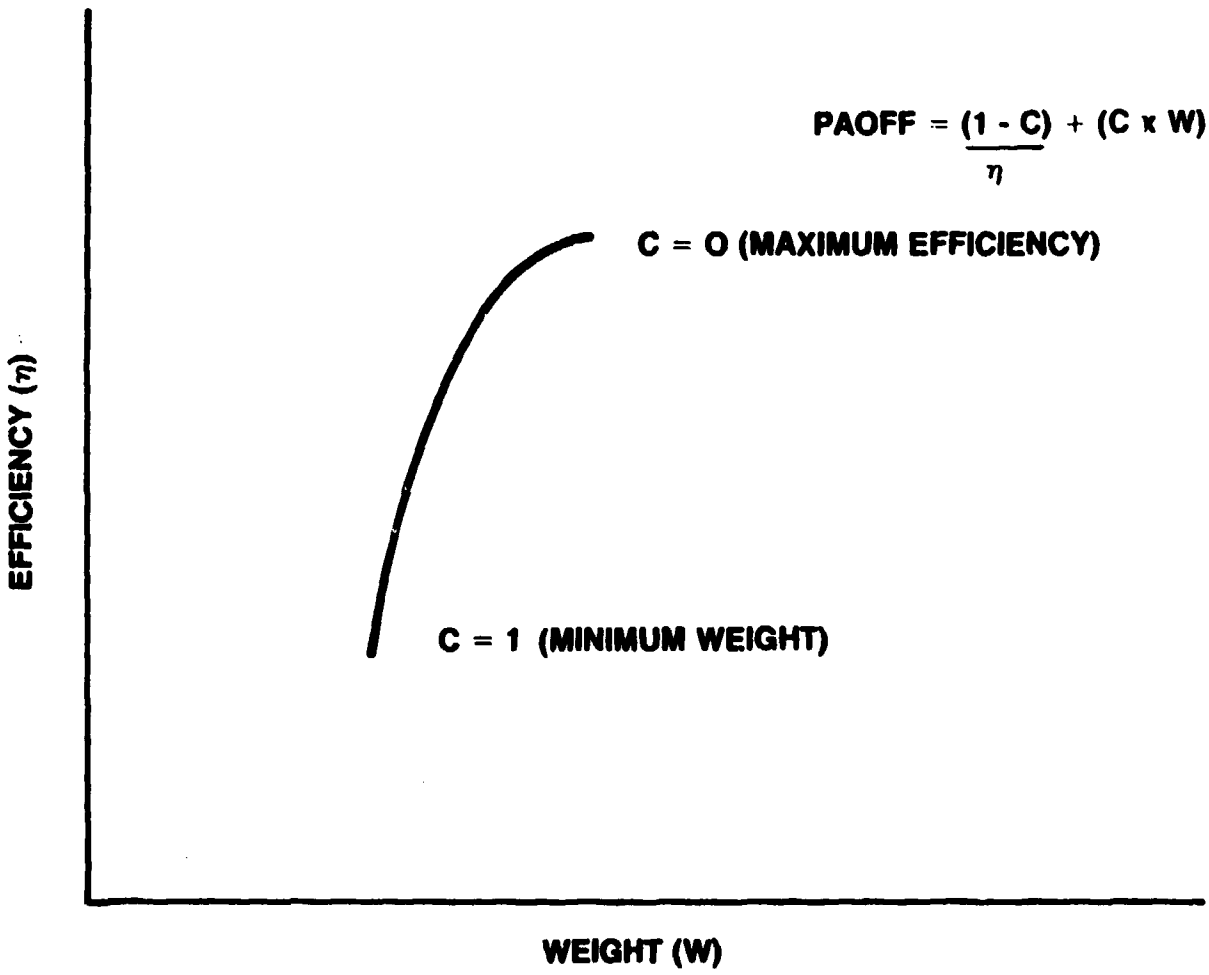

Figure 4 Generalized System Efficiency — Weight Characteristics

The use of values of C between zero and unity represent designs where appropriate weighting of system efficiency and weight applies. The multivariable optimization method uses a numerical technique for minimizing functions of many variables. This technique makes use of the slope-curvature method, utilizing both first and second numerically formed partial derivatives to determine optimum variable incrementation. The point on the surface of the function where the first partial derivative is zero is estimated by using the values of the first and second partial derivatives evaluated about a base point.

The optimizing technique consists of evaluating first and second partial derivatives for each optimizing variable at a base point on the surface of the PAOFF function. A search mode is then entered whereby each variable is incremented until the PAOFF function passes through a partial optimum. Then the point which resulted in this partial optimum is used as a new base point about which the procedure is repeated until the difference between successive base points is close to zero. The optimizing variables used are presented in Table I.

Table I Optimizing Variables

Variable	Turbine Type*	Specified Limits
Turbine Inlet Temperature	1, 2	450—815°C (842—1500°F)
Turbine Inlet Pressure	1, 2	6.89 — 17.23 MPa (1000—2500 PSIA)
Condenser Temperature	1, 2	38.3—148.9°C (100—300°F)
Regenerator Vapor Pressure Drop	1, 2	
Regenerator Liquid Pressure Drop	1, 2	
Regenerator Effectiveness	1, 2	
Fan Electrical Power	1, 2	
Condenser Effectiveness	1, 2	
Rotational Speed	1, 2	
Turbine Diameter	1, 2	
Turbine Arc of Admission	1	
Turbine Blade Height	2	
Turbine Pressure Ratio	2	

*Refers to number of turbine stages.

The limits placed upon the optimizing variables were determined from the contract Statement of Work and previous experience with similar systems. The turbine rotational speed was limited by alternator stress and critical speed considerations based upon previous alternator rotor designs.

The shape of the optimum curve shown in Figure 4 (representing a family of optimum systems) shows that at the maximum efficiency end of the curve, large increases in weight accrue for only small changes in performance. This may result, for instance, from an increasing condenser size to

reduce turbine backpressure. At the other end of the curve the opposite happens, large reductions in efficiency occurring for only small reductions in system weight.

Optimized system analyses were performed at fixed temperatures to allow the effect of temperature alone to be determined. System weight analyses were calculated based on the preliminary configuration shown in Figure 1. A summary of the design-point specification is given in Table II.

Table II Design Point Specification

Output Power	kW_e	15
Frequency	Hz	60
Voltage	V	120/208, 3-Phase
Power Factor		0.8
Design Life	Years	30
Annual Duty	Hrs	3300
Condenser		Air cooled
Ambient Air Temperature	°C	26.8 (80°F)
Receiver Pressure Drop (% of throttle pressure)		10
Minimum System Efficiency %		20

All calculations were performed in English units and these are presented in parentheses following the SI units.

3.2 SINGLE-STAGE STEAM TURBINE

Figure 5 shows the schematic used for the parametric analysis of the single-stage steam system. The results of the optimized system analysis as a function of turbine inlet temperature are shown in Figure 6, with fractional numbers referring to the weighting factor, C, selected. These results are summarized in Table III.

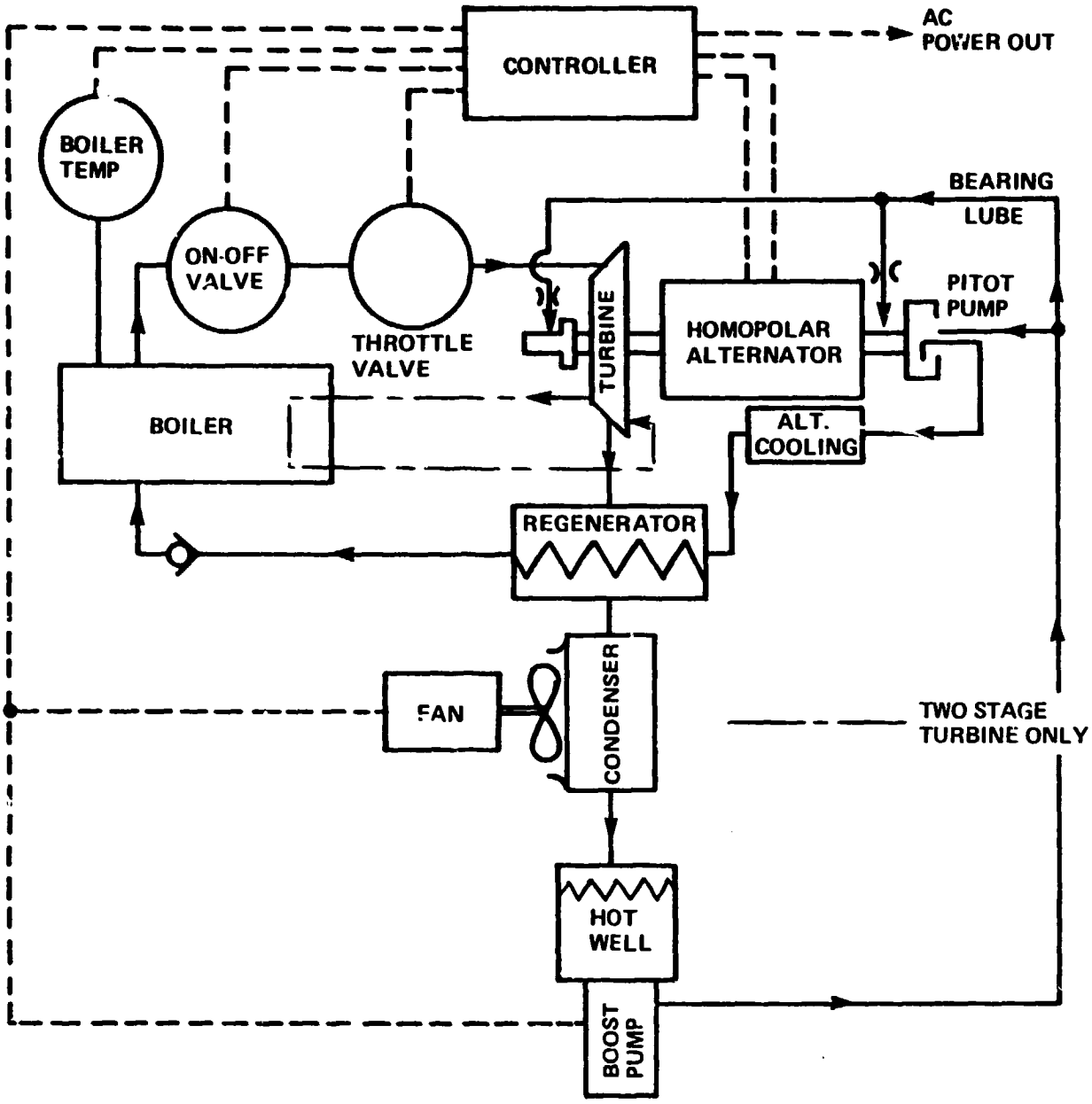

Figure 5 15 KW_e System Schematic

DOE/NASA/0061-79/1
NASA CR-159589
AER 1713

15 kWe (NOMINAL) SOLAR THERMAL ELECTRIC POWER CONVERSION CONCEPT DEFINITION STUDY — STEAM RANKINE TURBINE SYSTEM

Timothy Bland
Sundstrand Corporation

October 1979

Prepared for
National Aeronautics and Space Administration
Lewis Research Center
Under Contract DEN 3-61

for
U.S. DEPARTMENT OF ENGERY
Office of Solar, Geothermal, Electric and Storage Systems
Division of Central Solar Technology

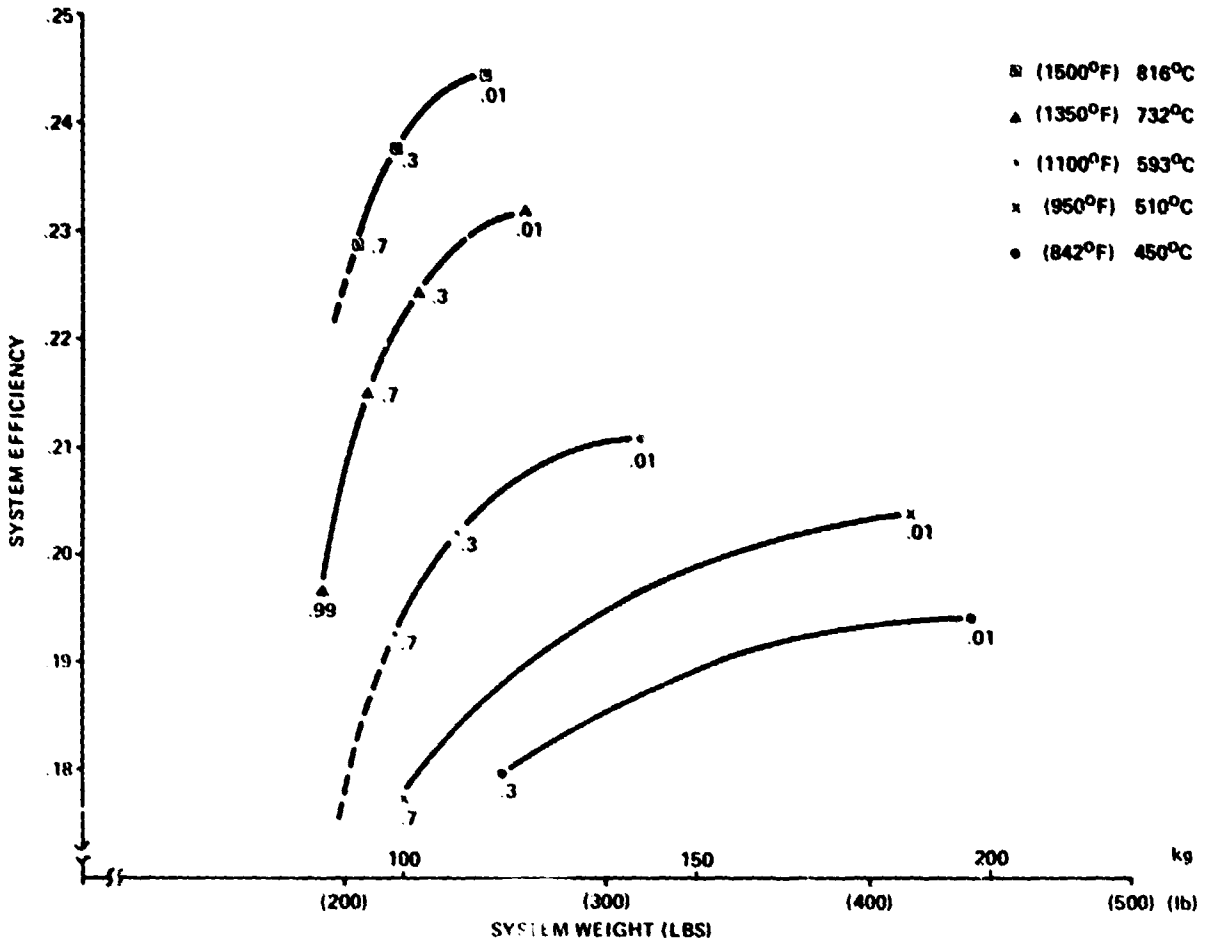

Figure 6 Optimized Efficiency — Weight Characteristics, 15 KW_e Single Stage System

Table III Single-Stage Steam System Characteristics

Turbine Inlet Temperature		Turbine Inlet Pressure		Condenser Temperature		Condenser Pressure		System Weight		System Efficiency	System Mass Flow	
°C	(°F)	MPa	(PSIA)	°C	(°F)	KPa	(PSIA)	Kg	(lb)	%	Kg/hr	(lb/hr)
HIGH EFFICIENCY DESIGN (C = .01)												
450	842	5.30	768	48.9	120	11.7	1.69	197	434	19.0	93.4	206
510	950	5.18	752	48.9	120	11.7	1.69	193	425	20.4	83.9	185
593	1100	5.70	827	58.3	137	18.5	2.69	142	312	21.0	80.7	178
732	1350	6.41	930	59.4	139	19.7	2.86	122	270	23.2	70.8	156
816	1500	6.67	967	60.6	141	20.3	2.94	118	254	24.5	65.3	144
LOW WEIGHT DESIGN (C = .7)												
510	950	6.28	912	73.9	165	37.2	5.4	100	221	17.7	101	223
593	1100	6.79	985	71.1	160	32.4	4.7	99.3	219	19.3	90.3	199
732	1350	6.55	950	68.9	156	30.3	4.4	94.8	209	21.5	77.1	170
816	1500	6.70	972	68.3	155	29.6	4.3	93.0	205	22.9	70.8	156

3.3 TWO-STAGE STEAM TURBINE

The two-stage steam turbine system was analyzed using the schematic of Figure 5. Two turbine types were investigated, a two-stage re-entry turbine and a two-wheel configuration. The efficiency of the latter was much lower due to the disc friction and scavenging losses of the first stage, so the re-entry type was selected for all further analysis. The re-entry turbine configuration is shown conceptually in Figure 7.

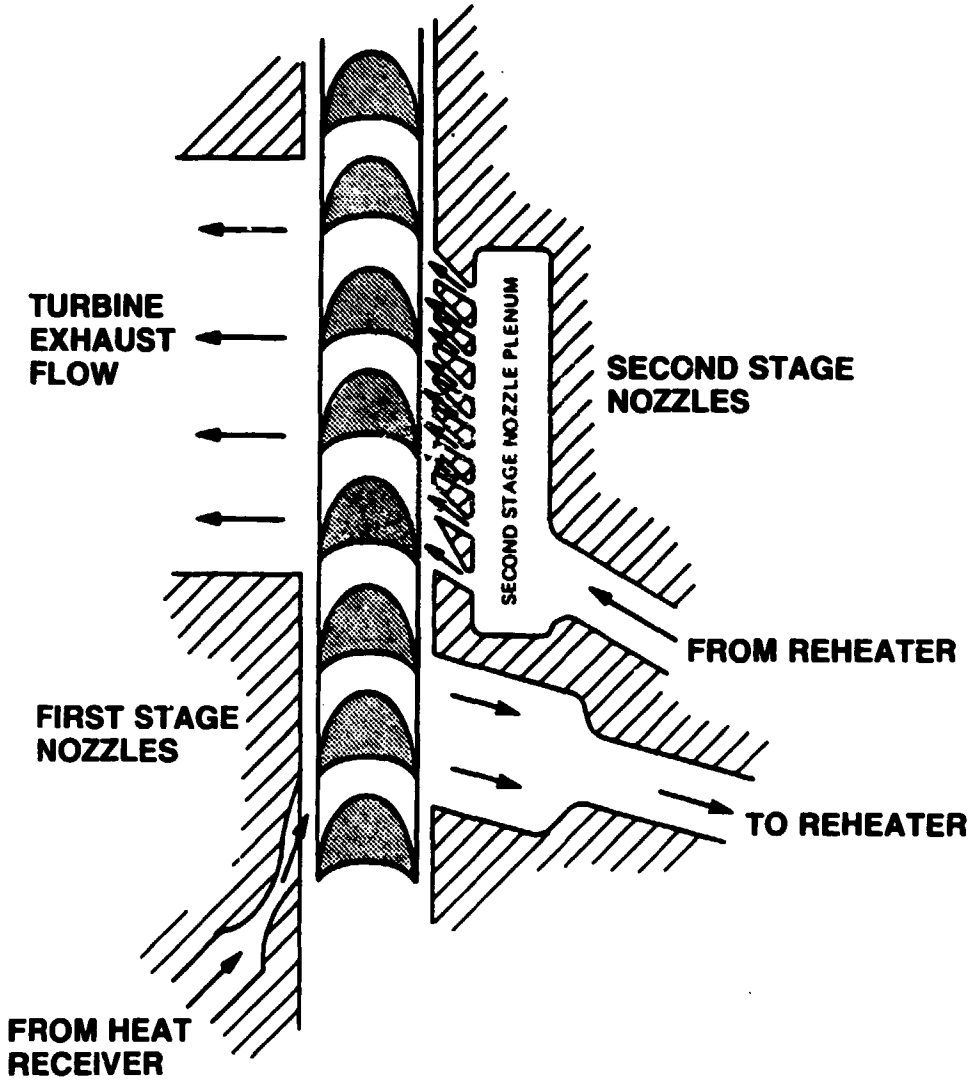

Figure 7 Two-Stage Re-entry Turbine Concept

The results of the optimized system analysis are shown in Figure 8 and summarized in Table IV for two selected turbine inlet temperatures. The two-stage design was optimized for blade height as well as for the pressure ratio split between first and second stages, rather than the arc of admission parameter used for the single-stage turbine. The most critical design consideration for the two-stage turbine is the axial clearance around the wheel for the first stage. Tight clearances minimize leakage from the first stage to the second stage exhaust. The analysis results presented in this section are for an axial clearance of 25.4 μm (0.001 inch). Preliminary design estimates showed that this clearance could be achieved by using a gas bearing support technique to separate the turbine wheel from the nozzle block. The effect of operating the turbine with larger clearances is shown in Figure 9, and it can be seen that by increasing the turbine clearance to 254 μm (0.010 inch) the system efficiency begins to approach that of a single-stage system.

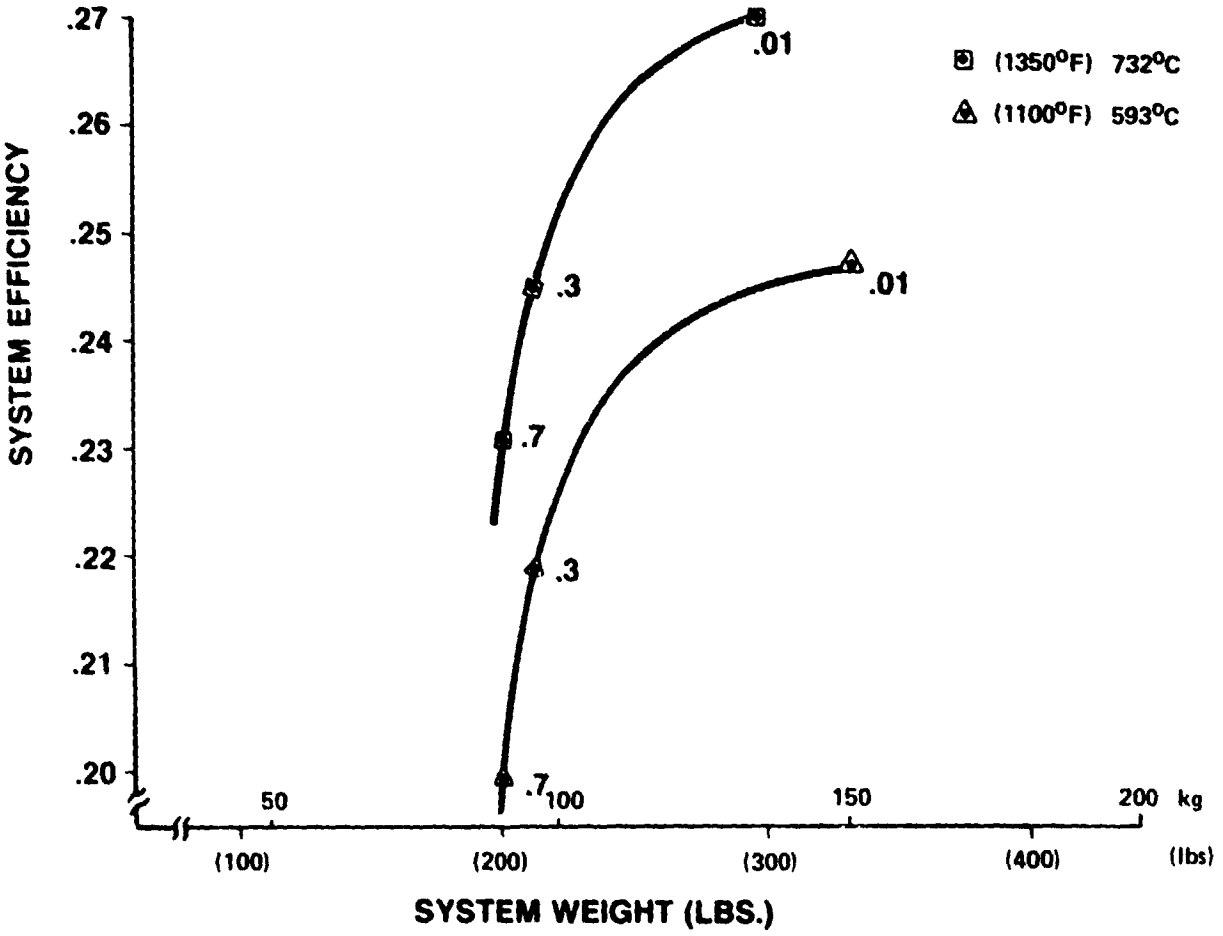

Figure 8 Optimized Efficiency — Weight Characteristics, 15 KW_e Single Stage System

Table IV Two-Stage Steam System Characteristics

Turbine Inlet Temperature		Turbine Inlet Pressure		Condenser Temperature		Condenser Pressure		System Weight		System Efficiency	System Mass Flow	
°C	(°F)	MPa	(PSIA)	°C	(°F)	KPa	(PSIA)	Kg	(lb)	%	Kg/hr	(lb/hr)
HIGH-EFFICIENCY DESIGN (C = .01)												
593	1100	3.79	550	48.9	120	11.7	1.69	150	331	24.7	62.6	138
732	1350	3.45	500	48.9	120	11.7	1.69	136	299	27.0	54.9	121
LOW-WEIGHT DESIGN (C = .7)												
593	1100	3.45	501	80.0	176	47.3	6.86	89.8	198	19.9	85.3	188
732	1350	5.17	750	80.6	177	47.3	7.0	91.2	201	23.1	70.3	155

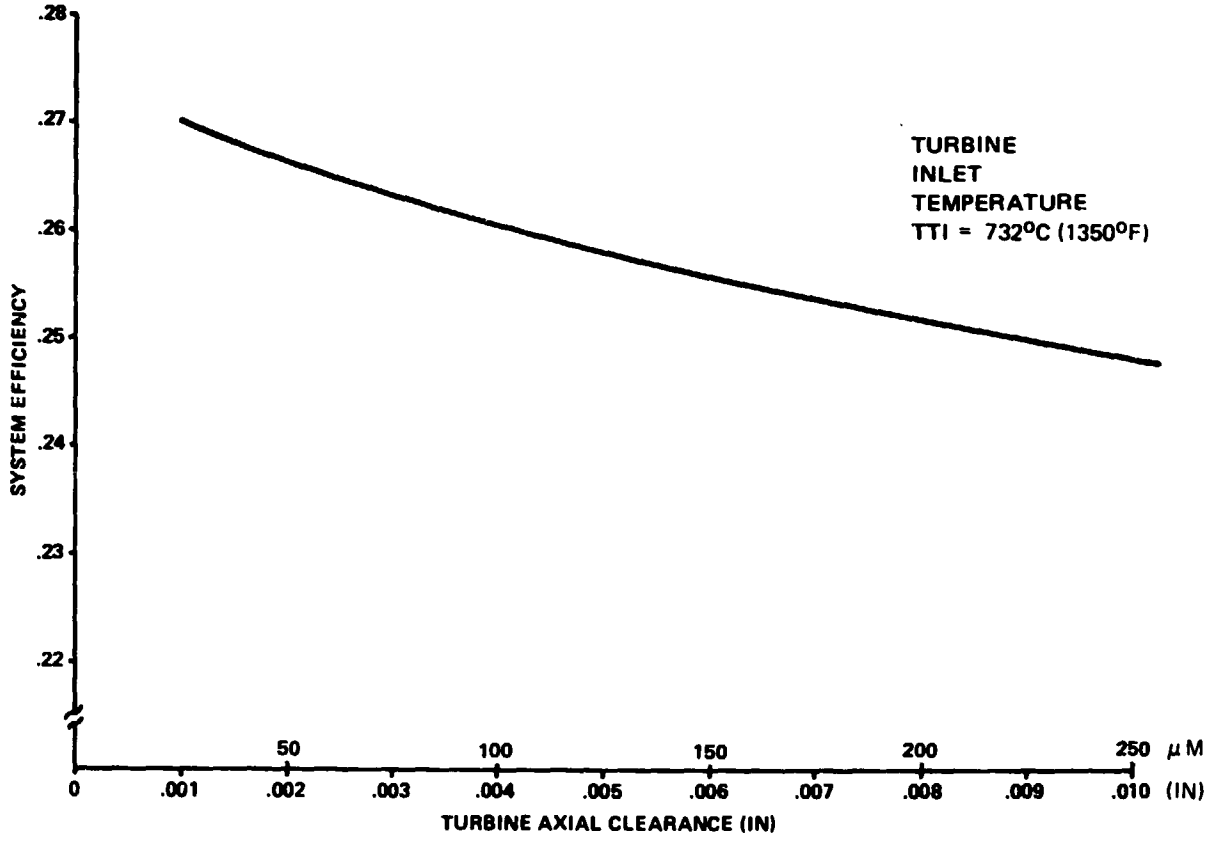

Figure 9 Optimized Two-Stage System Efficiency vs. Turbine Axial Clearance

3.4 SINGLE-STAGE TOLUENE TURBINE

In response to a specific NASA inquiry, preliminary analyses were performed of an organic Rankine cycle system. The single-stage schematic (Figure 5) was employed and Toluene (Methyl benzene) was selected as the working fluid. The organic system is highly regenerative in nature and this, combined with higher turbine efficiencies resulting from higher mass flows and lower isentropic head, gives system efficiencies about the same as the two-stage steam at much lower turbine inlet temperatures. A summary of the optimized, high-efficiency weighted system performance as a function of turbine inlet temperature is given in Table V.

Table V Toluene System Characteristics

Turbine Inlet Temperature		Turbine Inlet Pressure		Condenser Temperature		Condenser Pressure		System Weight		System Efficiency	System Mass Flow	
°C	(°F)	MPa	(PSIA)	°C	(°F)	KPa	(PSIA)	Kg	(lb)	%	Kg/hr	(lb/hr)
316	600	3.45	500	48.9	120	11.8	1.71	195	430	23.0	413	910
371	700	3.45	500	48.9	120	11.8	1.71	178	392	25.3	357	787
427	800	4.02	583	48.9	120	11.8	1.71	166	365	27.5	318	702

3.5 DISCUSSION OF RESULTS

The performance calculation results show that the two-stage steam turbine design with reheat results in significantly improved system efficiencies over the single-stage steam system. The use of an organic fluid allows similar high efficiencies to be achieved but at much lower temperatures and with the relatively simple single stage design. The Toluene operating temperature is limited to a maximum of 800°F due to fluid limitations.

The selection of the maximum cycle temperature which can be safely employed for long-life application in steam depends on the corrosion resistance of the selected materials. Tests of different boiler tube materials with high-temperature steam have been performed by the ASME Research Committee (Reference 8). These tests show that nickel-based alloys such as Inconel and Incolloy exhibit extremely low scale generation rates at 732°C (1350°F)(less than 25.4 μm (0.001 inch) in 18 months). Of the austenitic stainless steels only AISI 310 has rates as low as the nickel-based alloys; however, it should be noted that the strength of the stainless steel decreases considerably at this temperature. This is an advancement of the state-of-the-art since commercial steam systems limit their peak temperatures to 650°C (1200°F). It is to be assumed that adequate water treatment would be employed to limit the free oxygen content of the water to approximately 0.03 parts per million.

The achievement of reasonably high efficiencies with the two-stage re-entry steam turbine system is dependent on being able to develop a successful gas bearing system capable of allowing the turbine to operate with close axial clearances at high temperatures.

An overall summary of the parametric analysis results is presented in Table VI.

Table VI System Performance — Weight Summary (15 k_{w_e})

Turbine Inlet Temperature °F		STEAM						Toluene Single Stage		
		Single Stage			Two Stage With Reheat					
		Efficiency	Weight		Efficiency	Weight		Efficiency	Weight	
°C	°F	%	Kg	lb	%	Kg	lb	%	Kg	lb
427	800							27.5	166	365
450	842	19.0	200	440						
510	950	20.4	193	425						
593	1100	21.0	142	312	24.7	150	331			
732	1350	23.2	122	270	27.0	136	299			
816	1500	24.5	115	254						

4.0 CONCEPTUAL DESIGN

4.1 SYSTEM

The parametric analysis results indicated considerable improvement potential to be gained from the two-stage rather than the single-stage steam turbine. The study was therefore redirected to a conceptual design of a two-stage re-entry turbine version of the steam Rankine System with reheat between stages. The design point requirements given by NASA for this system are summarized in Table VII.

Table VII Two-Stage Design Point Requirements

Turbine Type	Two Stage Re-entry
Turbine Inlet Temperature	732°C (1350°F)
Thermal Input	80 KW
Heat Receiver Footprint	0.51m (20 in) Diameter Circle
Tracking Motion	Horizon To Horizon

The system design was re-optimized to meet the new thermal heat input requirements and the system was repackaged in an attempt to meet the heat receiver nominal dimension.

The complete system is shown in Figure 10, a summary of the system design point is given in Table VIII and a system schematic in Figure 11. The numbers on Figure 11 represent the system state points with pressures, temperatures, flow rates and enthalpies summarized in Table IX.

Following the hydraulic flow circuit from the boost pump, which is a high-speed, electrically-driven, hermetic, centrifugal pump, the condensate flow passes through the electronic controller where waste heat from the electrical conditioning circuits is absorbed. From here the liquid cools the turbine support housings and a small proportion of the flow is split off for lubricating the radial bearings before the remainder passes to the feed pump. The boiler feed pump, a single-stage pitot pump, pressurizes the water to the maximum pressure in the loop.

From the pitot pump the liquid passes through the flow control, or throttle valve and to the alternator where it picks up waste heat from the stator. From here the liquid passes into the inside of the finned-tube regenerator (feed water heater) where turbine exhaust superheat is absorbed before passing through the throttle valve to the vaporizer section of the receiver.

Steam from the receiver passes through the emergency on-off valve before expanding through the first stage of the re-entry turbine. High pressure steam is tapped upstream of this valve to provide flow to the hydrostatic steam thrust bearing.

The first stage exhaust is collected in a duct and returned to the receiver where it is reheated before returning to the second stage for a second pass through the turbine wheel; some first-stage inlet flow leaks directly to the second stage. The exhaust steam passes to the vapor side of the regenerator where it loses most of its superheat before passing into the bottom of the reflux, finned tube condenser. Here the steam condenses and drips into the hotwell before passing into the boost pump. The bearing lubricant drainage flow is ducted directly to the hotwell. During the start mode the boost pump pressurizes the start pump inlet which then provides adequate flow and pressure to pass liquid into the vaporizer even if still hot from recent operation. A system of check valves routes the flow in the correct direction when starting or running steady state and also provides back flow from the vaporizer on system shutdown. Figure 12 shows the main system power flow from the turbine shaft power to the useful 60 Hz electrical output. Figure 13 shows the heat rejection system defining the design point conditions.

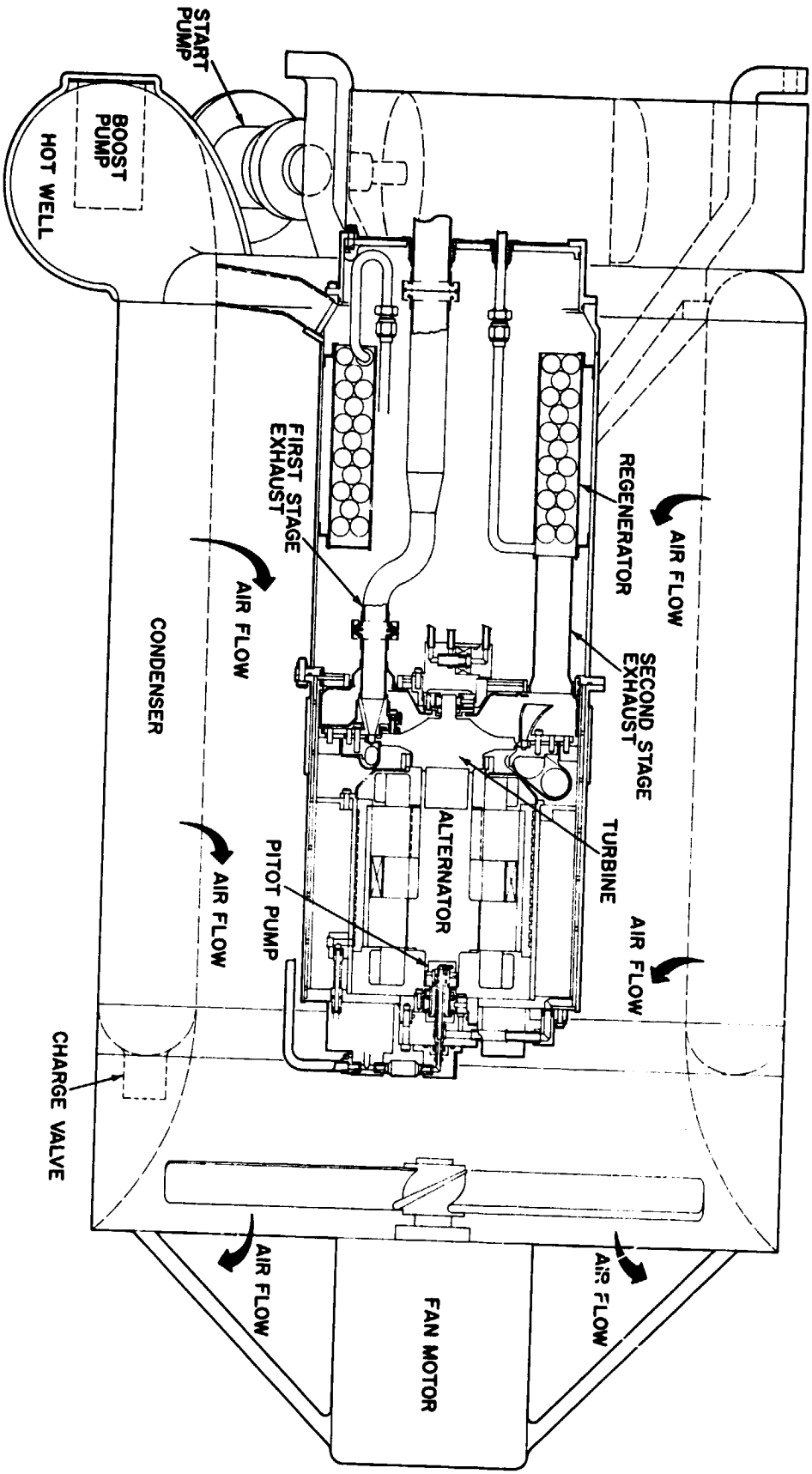

Figure 10 Two-Stage Steam Rankine System

Table VIII Two Stage Steam System Design Point (22 k_{W_e})

STATE POINTS			
Turbine Inlet Temperature — First Stage	°C	732	(1,350 °F)
Turbine Inlet Pressure — First Stage	MPa	4.13	(600 PSIA)
Reheater Inlet Temperature	°C	353	(668 °F)
Reheater Inlet Pressure	KPa	159.	(22.6 PSIA)
Turbine Inlet Temperature — Second Stage	°C	732	(1,350 °F)
Turbine Inlet Pressure — Second Stage	KPa	140.	(20.3 PSIA)
Condenser Temperature	°C	48.9	(120 °F)
Condenser Pressure	KPa	11.7	(1.69 PSIA)
Boiler Inlet Temperature	°C	257	(494 °F)
Boiler Inlet Pressure	MPa	4.61	(669 PSIA)
Heat Rejection Temperature	°C	26.7	(80 °F)
SYSTEM CHARACTERISTICS			
Rotational Speed	RPM	78,200	
Turbine Overall Efficiency		0.64	
Alternator Overall Efficiency		0.92	
Pump Efficiency		0.43	
Regenerator Effectiveness		0.97	
Condenser Fan Power	k_{W_e}	1.74	
System Weight	Kg	217	(478 lbs)
Thermal Input Power	k_W	8.0	
Net Output Power (60 Hz)	k_W	21.6	
System Efficiency		.27	
System Mass Flow	Kg/hr	81.2	(179 lb/hr)

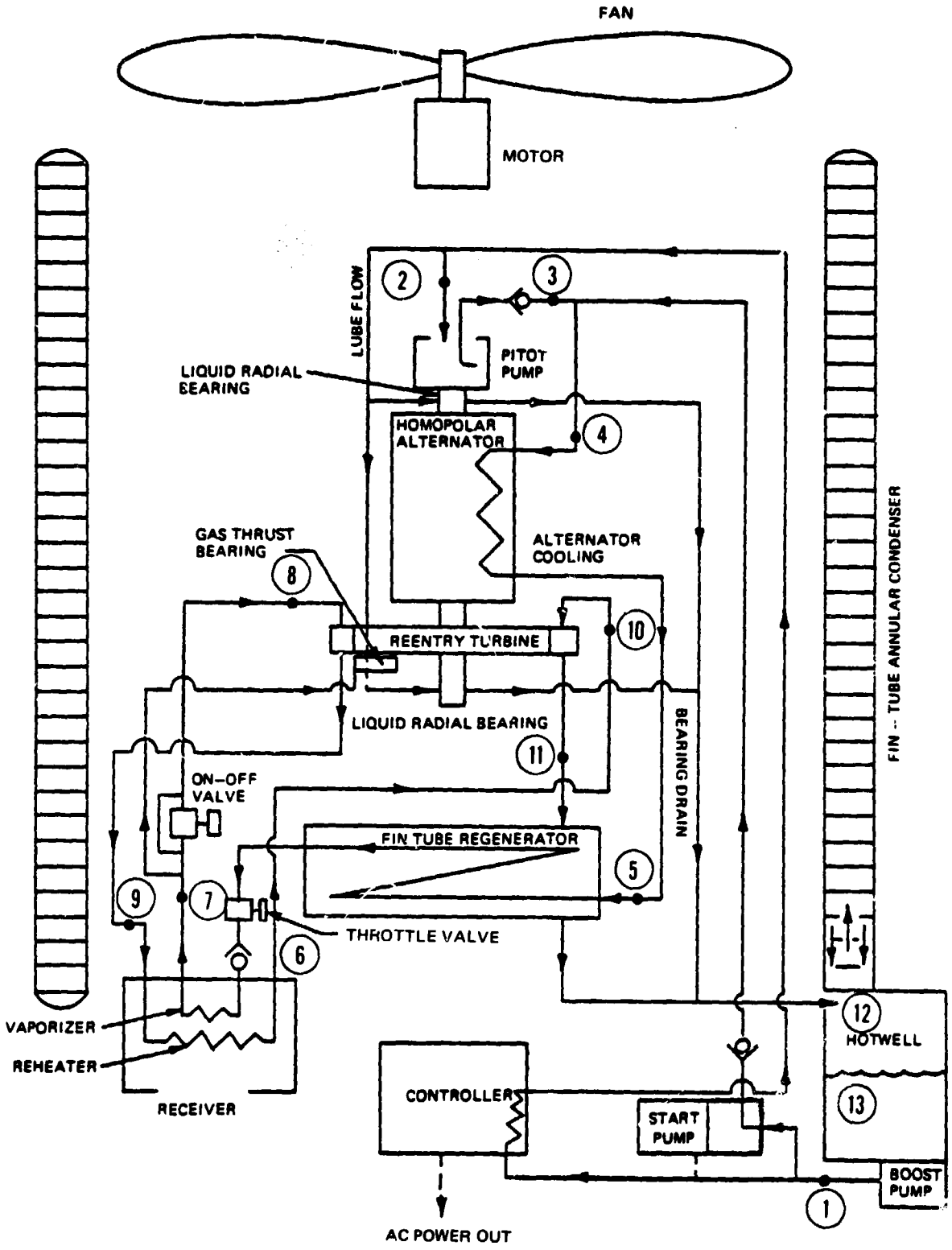

Figure 11 Two-Stage Steam Rankine Power System Schematic

Table IX System State Points (Refer to Figure 11)

Location	State Point	Pressure		Temperature		Enthalpy		Mass Flow	
		MPa	(PSIA)	°C	(°F)	J/Kg	(Btu/lb)	Kg/Hr	(Lb/Hr)
1	Boost Pump Outlet	.081	11.7	49.4	121	2.07×10^5	88.9	102	225
2	Feed Pump Inlet	.060	8.7	64.4	148	2.70×10^5	116	81.0	179
3	Feed Pump Outlet	4.66	676	67.2	153	2.82×10^5	121	81.0	179
4	Alternator Cooling Inlet	4.64	673	67.2	153	2.82×10^5	121	81.0	179
5	Regenerator Liquid Inlet	4.63	671	83.3	182	3.49×10^5	150	81.0	179
6	Vaporizer Inlet	4.61	669	257	494	1.12×10^6	481	81.0	179
7	Vaporizer Outlet	4.20	609	732	1350	3.98×10^6	1705	81.0	179
8	Turbine First Stage Inlet	4.13	599	732	1350	3.98×10^6	1705	81.0	179
9	Reheater Inlet	.156	22.6	353	668	3.18×10^6	1367	70.8	156
10	Turbine Second Stage Inlet	.140	20.3	732	1350	4.00×10^6	1718	70.8	156
11	Regenerator Vapor Inlet	.0123	1.79	482	900	3.05×10^6	1483	81.0	179
12	Condenser Inlet	.0117	1.69	95.6	204	2.68×10^6	1152	102	225
13	Condenser Hotwell	.0117	1.69	48.9	120	2.05×10^5	87.9	102	225

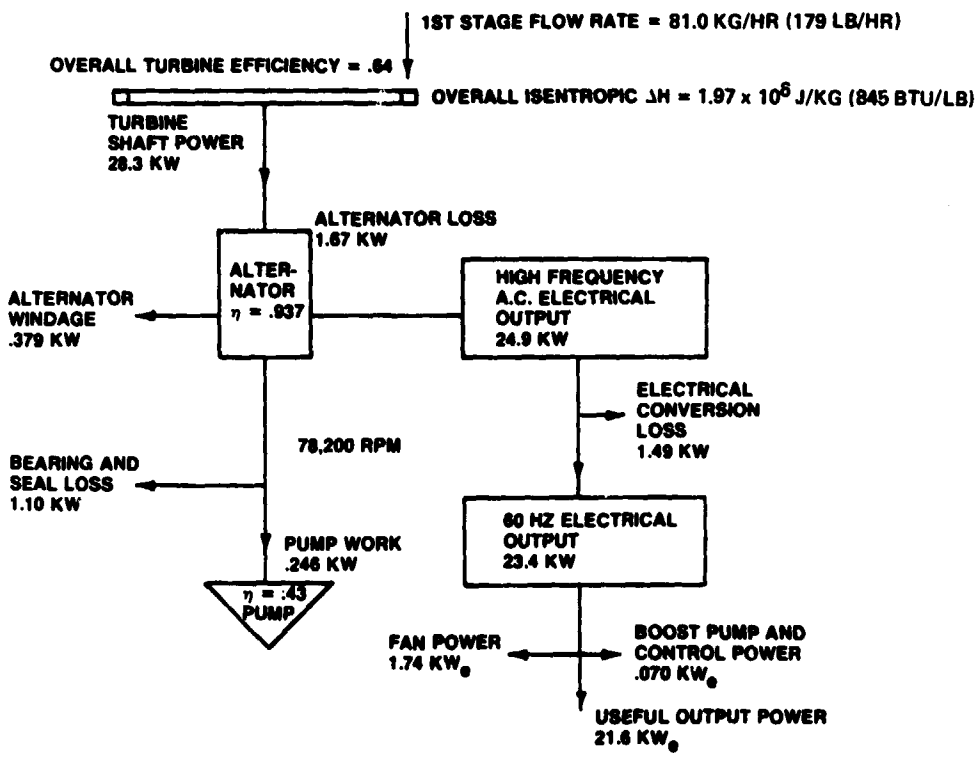

Figure 12 Two-Stage Power Flow Chart

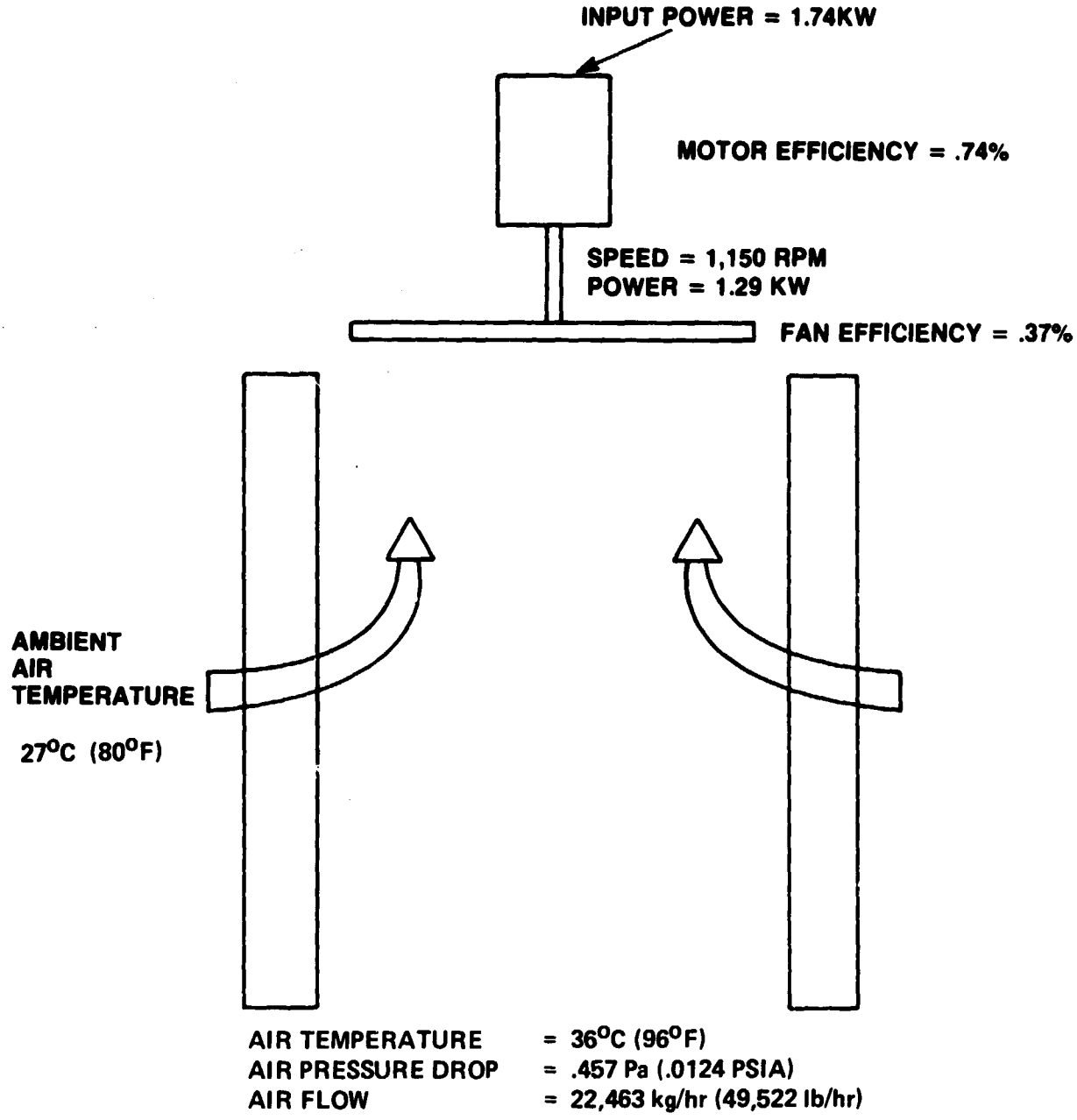

Figure 13 Heat Rejection System

4.2 COMBINED ROTATING UNIT (CRU)

The use of a CRU configured engine eliminates system-ambient dynamic seals and thus allows completely hermetic operation.

As shown in Figure 14, the combined rotating unit (CRU) comprises a re-entry turbine wheel, alternator rotor and pitot pump supported on tilting-pad, liquid-lubricated, radial bearings and a steam hydrostatic thrust bearing. The total CRU assembly includes the alternator stator, pump housings, turbine nozzle and exhaust blocks and associated support housings. The basic design principle is to provide water-cooled housings as a stable support base for the radial bearings at the turbine end and for the gas bearing/nozzle block assembly. This technique guarantees basic location of these components even while undergoing the thermal transients to operating temperature during startup.

The nozzle block/exhaust housing assemblies are mounted to the cold cylinder wall in three-point-mount arrangements which provide axial rigidity and thermal isolation but still allow free thermal growth. This is provided using spacers supported on three pins. One pin is tight, the second allows freedom of growth in one direction (thus maintaining circumferential location), and the third merely keeps the axial spacer in position, with completely free transverse motion. This may be seen in Figures 15 and 16. The spacers comprise a set of small ceramic washers, match-machined to the same height for one nozzle block/exhaust housing assembly. By selectively choosing the thickness of each set of spacers, the two nozzle block assemblies can be located in the same plane. Mounting the exhaust housing, rather than the nozzle block, to the cold wall minimizes heat transfer.

The nozzle blocks are mounted to their respective exhaust housings in the same manner. In this case the spacer thickness is selected to give the required total operating axial clearance across the turbine wheel. The cold clearance at assembly is chosen to allow for differential expansion, resulting in the correct hot operational clearances. The assemblies are each held together with a bolt located within the triangle formed by the three pins. Tension is maintained on the bolt by a belleville washer, thus allowing free lateral movement while maintaining axial location. This is shown in Figures 15 and 16.

4.2.1 Turbine

The turbine design is a two-stage, re-entry, supersonic, partial-admission, impulse type with 149 electro-chemically machined blades. Tight axial clearances of 38.1 μm (0.0015 inches) are maintained on each side of the wheel of the first stage. The selection of this clearance was based upon transient thermal analyses. A tip shroud with radial knife edges is brazed to the blades and cuts into a honeycomb tip seal during startup. This minimizes gas leakage across the top of the wheel. The tight axial clearances are necessary to minimize gas leakage from the first stage to the second stage. Leakage is not a problem in the second stage and hence larger clearances, 254 μm (0.010 inches), were selected here. This minimized tolerance problems associated with the much greater arc of admission of the second stage (65.4%). The turbine nozzles are conical in shape with a smoothly rounded entrance to the throat region. A summary of the geometry is presented in Table X.

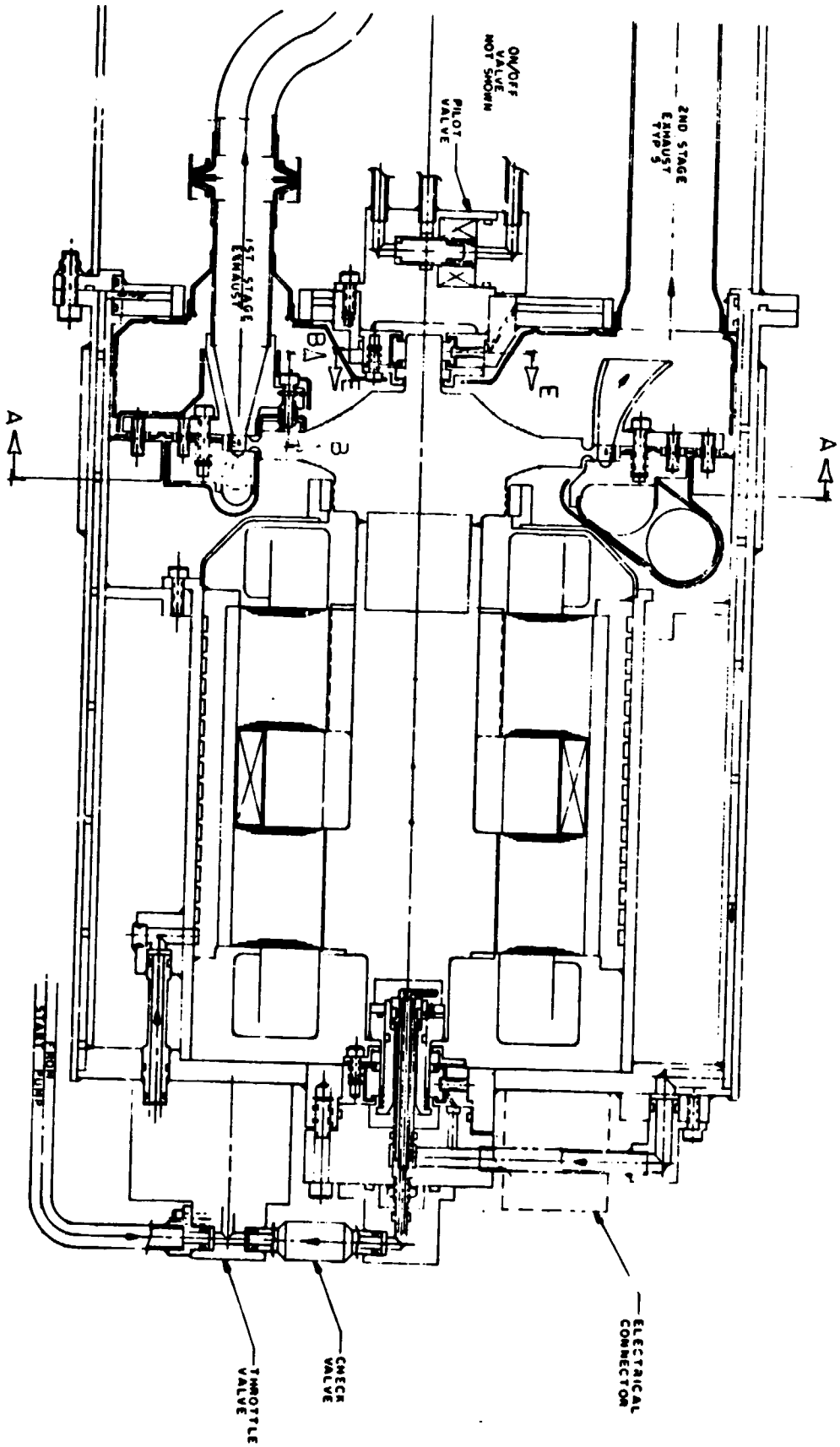

Figure 14 Combined Rotating Unit

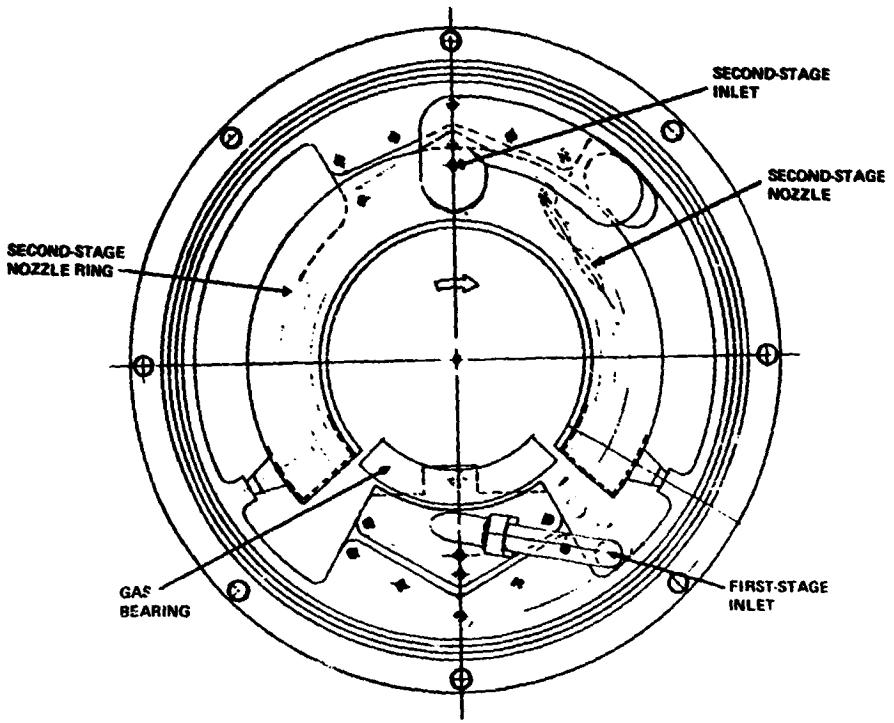

Figure 15 Turbine Housing Design

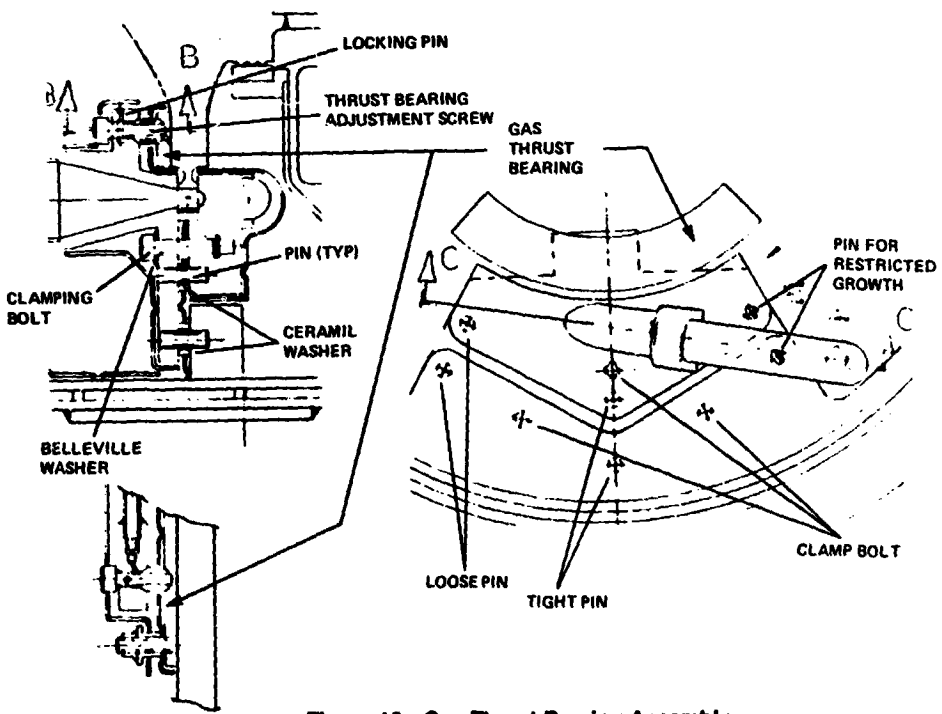

Figure 16 Gas Thrust Bearing Assembly

Table X Turbine Summary

Rotational Speed	RPM	78,200	
Diameter	Cm	15.67	(6.17 in)
Chord	Cm	.64	(.25 in)
Blade Height	Cm	.64	(.25 in)
First Stage Arc	%	4.3	
Second Stage Arc	%	65.4	
Number of Nozzles — First Stage		1	
Number of Nozzles — Second Stage		15	
Velocity Ratio — First Stage		.44	
Velocity Ratio — Second Stage		.48	
Overall Efficiency		.64	

The need to provide a flat radial surface for the gas bearing resulted in a wide wheel to satisfy stress requirements. The wheel design criterion was for burst at 150% overspeed. Based on experience and the calculated stress numbers the mode of failure was predicted to be one in which the turbine blades peeled off the disc rather than a disc burst. Consequently the containment requirements are for blade fragments only, resulting in a slightly increased wall thickness requirement in the form of a local 'belly band' around the outer housing.

Thermal analysis results were used for determining the wheel temperature at different radial locations, and these were used for calculating thermal stresses and material strength properties. Stress calculations were made at 110% overspeed which was considered to be the maximum normal operating speed. At this condition the lowest safety factors are 10% on yield and 30% on ultimate strength.

A preliminary thermal analysis was performed of the turbine area in order to predict steady state and transient component temperatures. These were used for material selection and to determine safe operating clearances for the turbine wheel. Calculated bearing, turbine disc friction and pumping losses were incorporated and estimates made of the bearing and alternator boundary conditions. Appropriate heat transfer coefficients for the turbine wheel and gas bearing were incorporated. Heat shields were used to minimize radiative heat transfer from hot turbine housings to cool support housings, while ceramic spacers were used to minimize conductive heat transfer between housings.

The transient analysis was based on a step increase in turbine inlet flow and temperature. A final system design would need better definition of the input conditions as a function of time. Figure 17 shows some selected nodes used for the analysis and Table XI gives transient and steady state temperatures for these nodes.

Individual housings were generally treated as isothermal in order to limit the number of analysis nodes. This is a good approximation where thermal isolation is effective. Detailed design analysis would require many more analysis nodes to determine thermal gradients within each component. The transient analysis calculations were used to determine the transient differential growth characteristics of the first stage nozzle block assembly in order to evaluate the minimum acceptable operating clearance.

Heat losses within the CRU and throughout the system were not included in the cycle analysis. Detailed analysis of the leakage paths and magnitudes would be necessary for a final design and these would impact performance slightly.

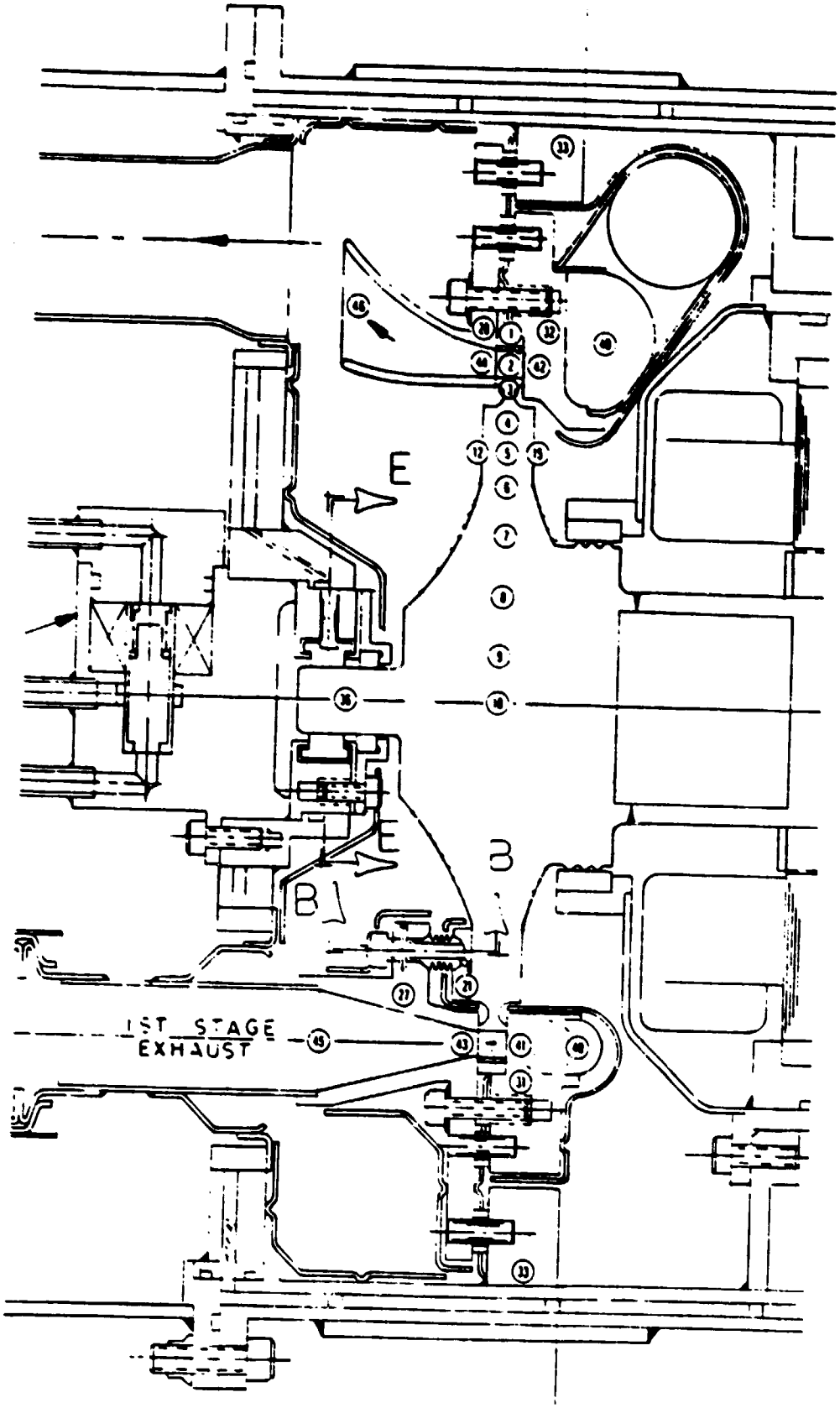

Figure 17 Thermal Model Map

Table XI Thermal Analysis Results

Node Number	Node Description	Temperature °C (°F)											
		5 Secs		10 Secs		30 Secs		2 Min		10 Min		Steadystate	
1	Turbine Wheel Shroud	357	(675)	375	(707)	371	(699)	412	(773)	460	(860)	492	(917)
2	Turbine Blades	353	(667)	376	(708)	372	(702)	417	(782)	464	(868)	491	(915)
3	Turbine Blade Root	128	(262)	195	(383)	265	(509)	387	(728)	510	(950)	568	(1055)
4	Gas Bearing	48.9	(120)	87.8	(190)	187	(368)	364	(688)	550	(1022)	637	(1179)
5	Gas Bearing	41.1	(106)	65.6	(150)	151	(303)	338	(640)	554	(1029)	656	(1213)
6	Gas Bearing	39.4	(103)	56.7	(134)	117	(243)	287	(549)	533	(991)	655	(1211)
7	Turbine Wheel	28.9	(84)	37.2	(99)	67.2	(153)	199	(390)	481	(898)	632	(1170)
8	Turbine Wheel	24.4	(76)	27.8	(82)	40.0	(104)	127	(261)	439	(822)	619	(1147)
9	Turbine Wheel	21.7	(71)	22.2	(72)	28.3	(83)	94.4	(202)	417	(783)	614	(1137)
10	Turbine Wheel	21.1	(70)	21.1	(70)	23.9	(75)	38.9	(102)	399	(751)	609	(1129)
12	Gas Bearing	58.9	(138)	82.2	(180)	162	(323)	345	(653)	556	(1033)	657	(1214)
15	Gas Bearing	82.2	(180)	106	(222)	184	(364)	368	(695)	579	(1075)	679	(1254)
21	Gas Bearing Pad	58.3	(137)	95	(203)	214	(418)	512	(953)	718	(1324)	774	(1426)
27	1st Stage Exhaust Housing	33.9	(93)	46.7	(116)	72.2	(162)	166	(331)	350	(662)	397	(747)
28	2nd Stage Exhaust Housing	23.3	(74)	26.1	(79)	33.9	(93)	70.6	(159)	226	(439)	462	(864)
31	1st Stage Inlet Housing	30.6	(87)	40.6	(105)	77.8	(172)	222	(432)	558	(1037)	644	(1191)
32	2nd Stage Inlet Housing	25.0	(77)	29.4	(85)	45.6	(114)	115	(239)	363	(686)	623	(1153)
33	Cold Wall	21.1	(70)	21.1	(70)	21.7	(71)	22.8	(73)	30.0	(86)	48.9	(120)
36	Bearing Journal	21.1	(70)	21.1	(70)	21.7	(71)	23.9	(75)	33.9	(93)	60.0	(140)
40	Inlet Gas	732	(1350)	732	(1350)	732	(1350)	732	(1350)	732	(1350)	732	(1350)
41	1st Stage Nozzle Exit Gas	719	(1327)	720	(1328)	721	(1329)	723	(1334)	729	(1344)	731	(1347)
42	2nd Stage Nozzle Exit Gas	717	(1322)	717	(1322)	717	(1323)	718	(1325)	724	(1335)	729	(1345)
43	1st Stage Diffuser Inlet Gas	697	(1287)	662	(1223)	332	(629)	334	(634)	341	(646)	342	(647)
44	2nd Stage Diffuser Inlet Gas	706	(1303)	679	(1254)	467	(873)	468	(875)	474	(885)	479	(895)
45	1st Stage Diffuser Exit Gas	684	(1264)	650	(1202)	327	(620)	331	(628)	341	(646)	343	(649)
46	2nd Stage Diffuser Exit Gas	699	(1291)	673	(1243)	463	(865)	464	(868)	471	(880)	479	(894)

4.2.2 Alternator

The alternator is a homopolar, inductor type. A four-pole rotor rotates within the stator formed by two stacks of laminations connected by a magnetic back iron and incorporating three-phase power windings passing through slots in the laminations. The alternator is excited by a field coil located between the lamination stacks and powered by the controller. Waste heat from the alternator stator is removed by passing system flow through cooling channels in intimate contact with the magnetic back iron or yoke.

The stator laminations are made of silicon iron and are 127 μm thick (0.005 inches) with 27 slots for the main winding. Both laminated and solid rotor poles were investigated and it was found that laminations gave only a marginal improvement in performance, but presented considerable manufacturing and stress problems. For this reason the solid rotor was selected with a design-point electro-magnetic efficiency of 93.7%. Windage losses reduce this to an overall

efficiency of 92.4%. Figure 18 gives performance predictions for the alternator as a function of power level. It should be noted that maximum output power capability decreases with decreasing speeds due to magnetic saturation and that windage losses also decrease with reduced speed, resulting in a fairly constant efficiency.

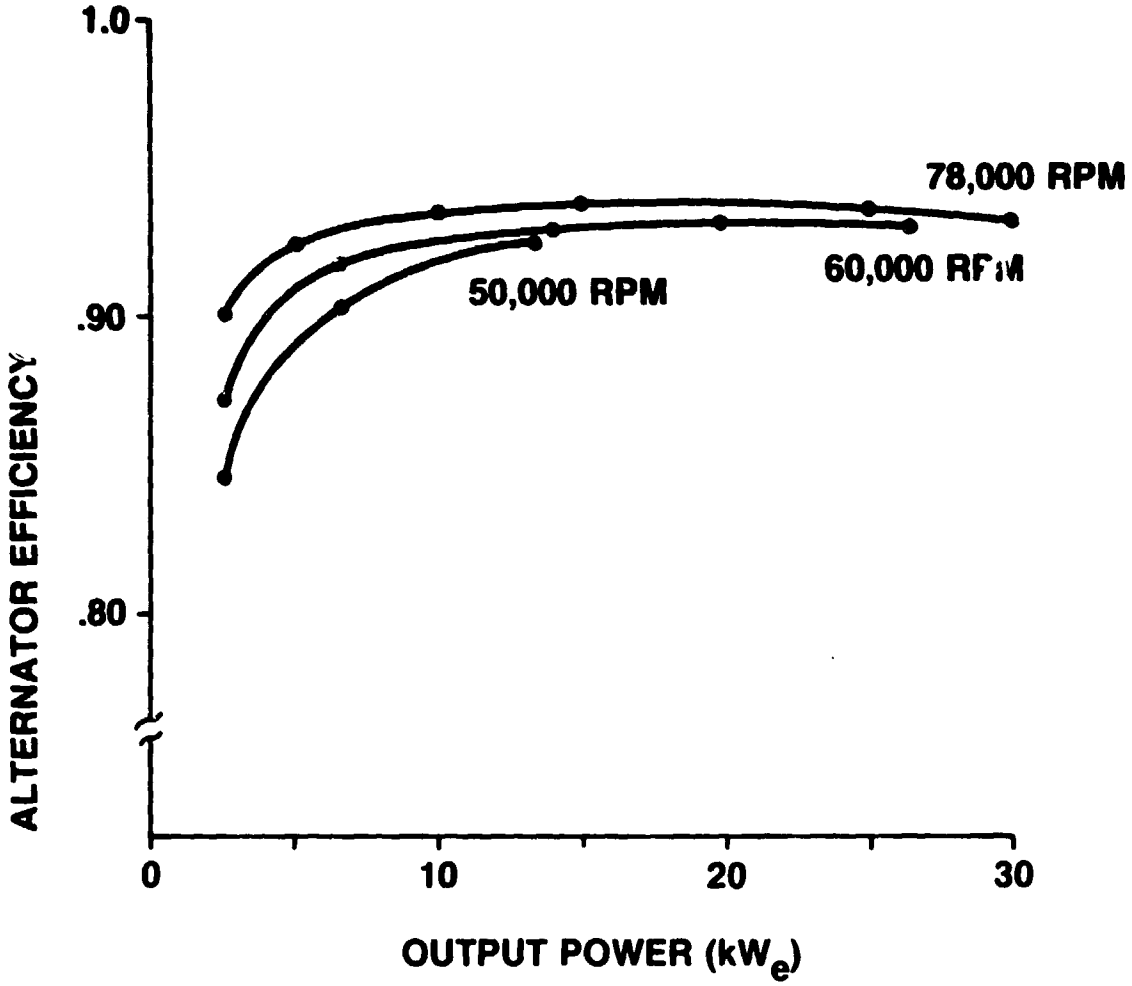

Figure 18 Alternator Electromagnetic Efficiency vs. Output Power

4.2.3 Feed Pump

The feed pump, shown in Figure 19, is a pitot pump in which a pitot probe is immersed in a rotating housing. Inlet flow is pumped through radial holes in the rotating housing and then passes into the throat of the stationary probe where dynamic head is recovered. Seals prevent inlet flow from leaking into the bearing cavity. The radial bearing surface is formed by welding the pump housing into the rotor. The probe and seal assembly then passes through the inner diameter of the shaft. The probe may be constructed in two ways, either by an electro-discharge machining process through the bottom of the probe, followed by the plugging of the access hole, or alternatively by an investment casting procedure.

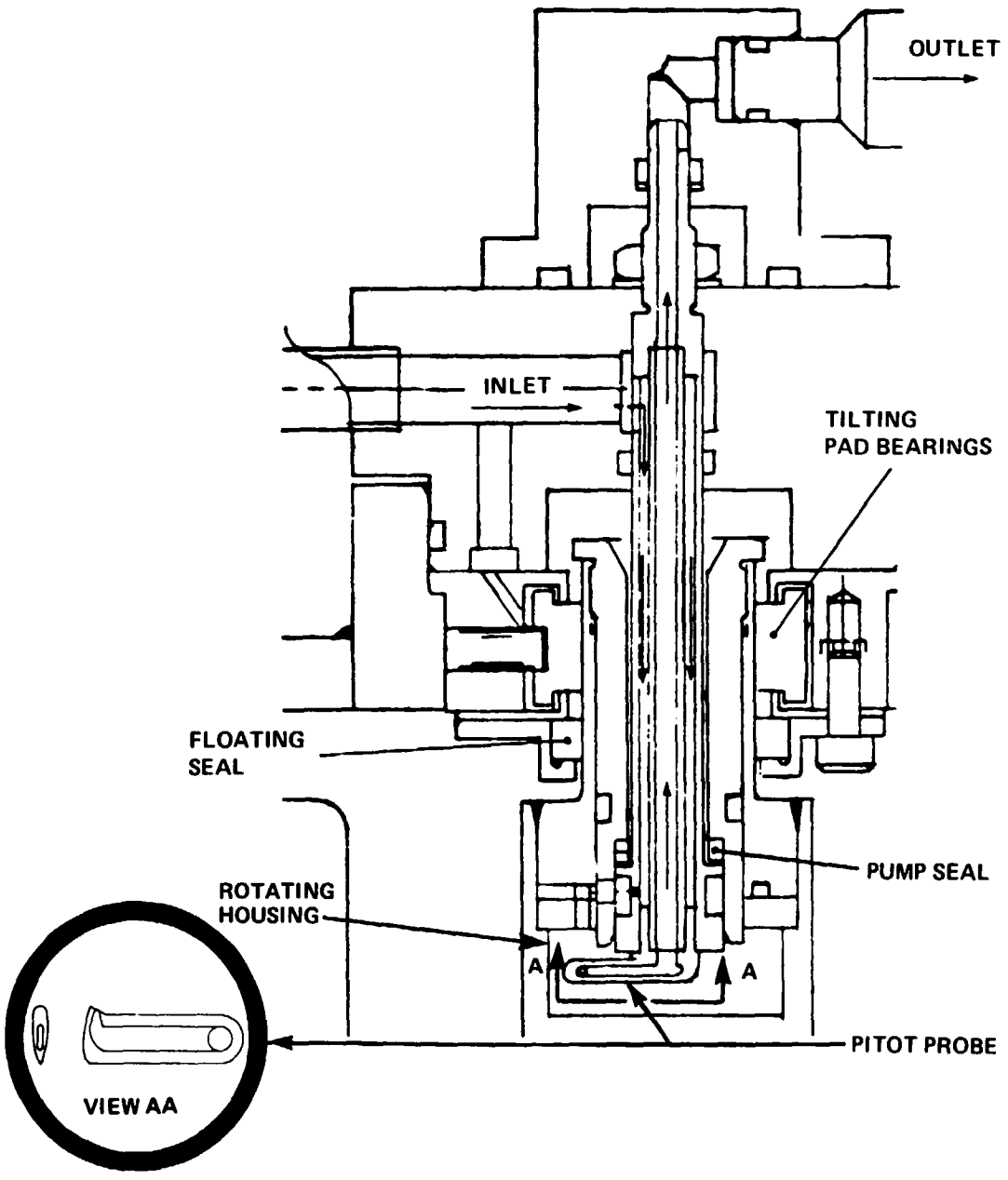

Figure 19 Pitot Pump

In either case a one-piece probe is constructed. The exterior probe shape is critical to the good performance of the pump. The performance of the pump is based on empirical efficiency-specific speed data, leading to a design point efficiency of 43%. The pressure rise-flow characteristics for the pump are presented in Figure 20.

4.2.4 Thrust Bearing

A gas bearing was essential to the ability to hold tight axial clearances around the turbine wheel thus minimizing interstage leakage and maximizing turbine efficiency.

It should be noted that with the unidirectional gas flow through the turbine (Figure 21) a unidirectional thrust load was guaranteed, comprising the sum of gravity loads, system pump pressure loading and turbine thrust load. This allowed the use of a single thrust bearing with a large savings in power loss.

Various configurations of self-acting bearings were investigated including resiliently-mounted bearings and compliant surface (foil) bearings. The self-acting bearing was assumed to occupy a partial arc of the turbine housing. The very low ambient pressure of 12.3 KPa (1.79 psia) led to difficulty in achieving analytical solutions, but a bearing design with 11.43 cm (4.5 inches) O.D. and 8.89 cm (3.5 inches) I.D. had a load capacity of approximately 13.3 N (3 pounds) at 10 μm (0.004 inches) film thickness, 57.8 N (14 pounds) at 2.54 μm (0.0001 inches). However, the estimated inertial load associated with a total axial turbine wheel runout of 2.54 μm (0.0001 inches) was approximately 16 g's to 854 N (192 pounds) leading to the conclusion that the self-acting bearing was inadequate.

A hydrostatic steam bearing was therefore selected, comprising a circumferential groove cut almost to the ends of the 90^0 partial arc pad shown in Figure 22. This groove is supplied with steam via an orifice upstream of the groove to control the flow. The design calculations were based upon selecting an orifice that would choke at axial bearing clearances greater than 12.7 μm (0.0005 inches), i.e., average operating film thickness.

The bearing was designed to operate with a minimum film thickness of 12.7 μm (0.0005 inches) at the maximum load condition, i.e., with the unit in the near vertical position at noon. At lower loads the film thickness is greater. The bearing clearance is set at assembly to accommodate thermal differential transient growth and achieve equal operating clearance on both sides of the turbine wheel at the maximum load point.

The calculated flow rate was extremely low and would not impact system performance, but would require a relatively small orifice. A Visco-jet was incorporated rather than a small drilled hole, eliminating concern for blockage by contamination.

The hydrostatic supply to the gas bearing is supplied directly from upstream of the main steam shutoff valve and thus is always pressurized before and after startup and shutdown. The steam is ducted around the pivot support using a bellows arrangement.

The need for a radial land on the turbine wheel for the gas thrust-bearing operating surface resulted in additional thickness being required to meet the wheel stress criteria. With a blade chord length of 0.635 cm (0.25 inches) this resulted in a stepped wheel configuration. The manufacturing tolerances required to produce a stepped wheel and matching stepped housings precluded the capability of operating with the necessary tight axial wheel clearances using a rigidly mounted gas bearing/exhaust housing assembly.

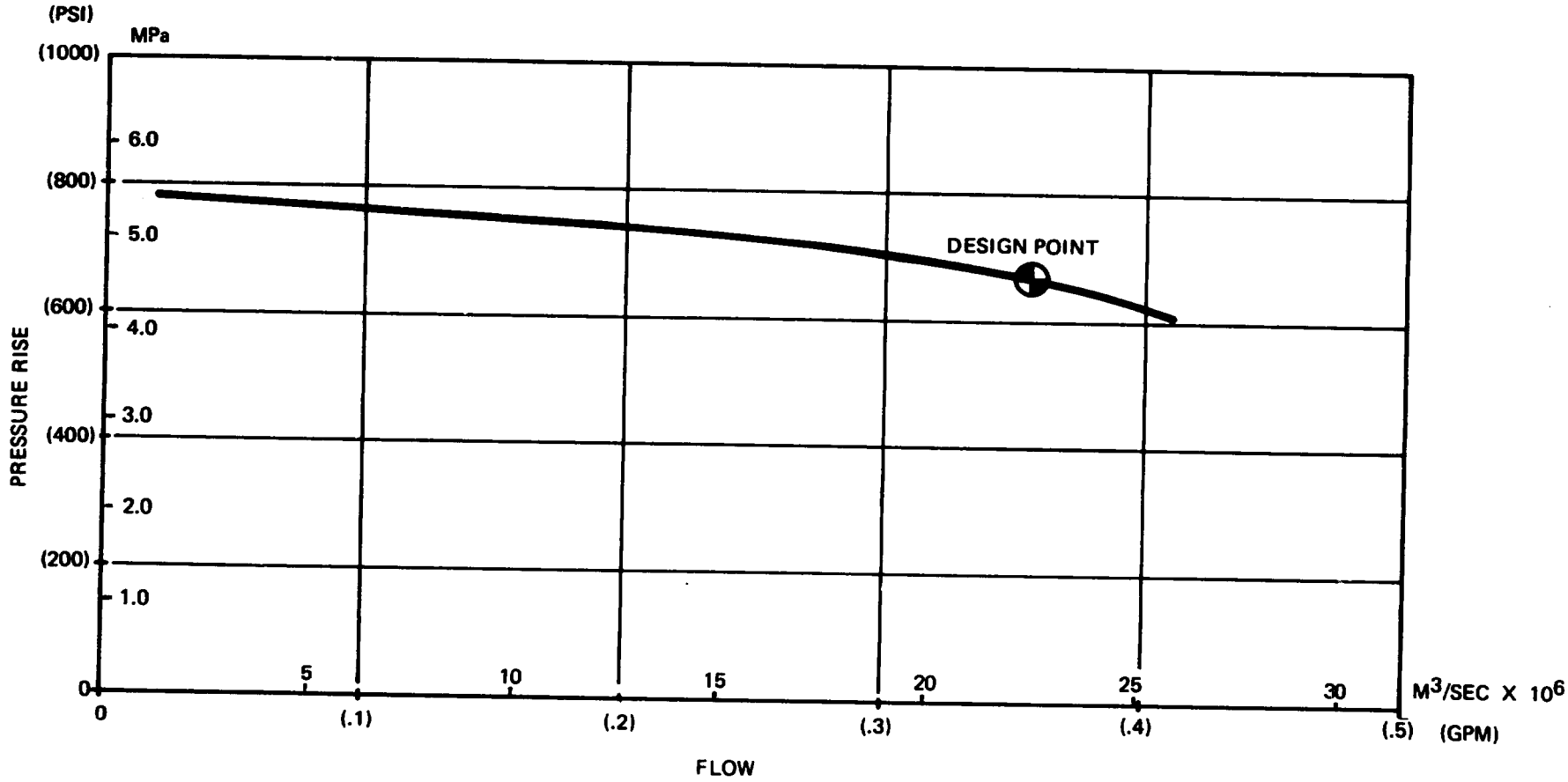

Figure 20 Pitot Pump Pressure — Flow Characteristics

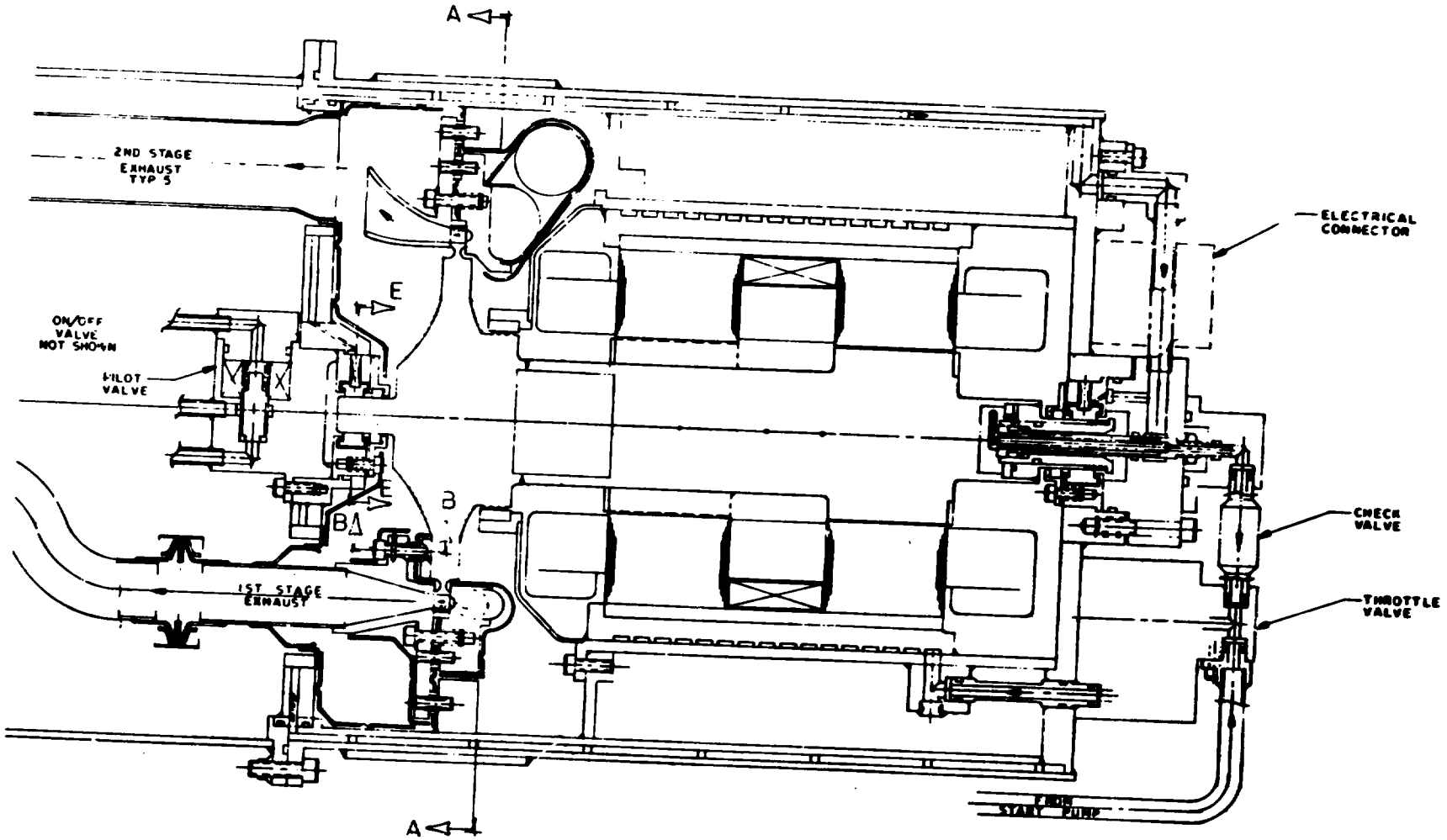

Figure 21 Combined Rotating Unit

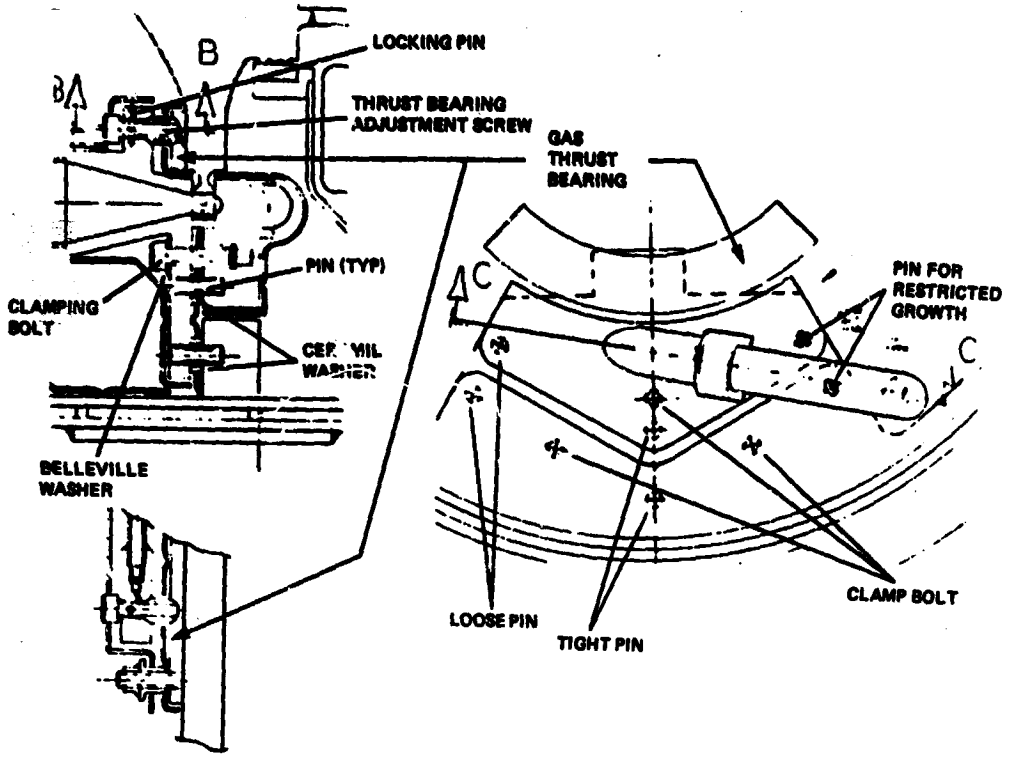

Figure 22 Gas Thrust Bearing Assembly

To overcome the difficulty of using rigid thrust bearings, the thrust bearing has been mounted with a pivot, like a tilting pad bearing, with the capability of axial adjustment to enable the required operating clearances around the turbine wheel to be obtained. The pivot mount can accommodate angular misalignment resulting from manufacturing tolerances. The assembly procedure would employ shims to locate the wheel centrally within the clearance space and another shim would then be positioned in the bearing clearance. The thrust bearing pad would then be tightened to the correct location and a locking pin inserted through the adjustment screw. This can be seen in Figure 22.

The axial critical speed associated with the axial stiffness at zero eccentricity is approximately 7000 rpm. This value is far removed from the normal operating speed range and the rotor will accelerate very rapidly through the critical speed precluding the potential for excessive amplitudes. A stiffness of greater than 350 X 10^6 N/m (2 million lb/inch) would be necessary to remove the critical speed above the design operating point. The bearing would have poor damping if the groove depth were shallow, whereas a deep groove would lead to pneumatic hammer problems, therefore, additional damping may be necessary. This may be obtainable from the pitot pump or from the radial liquid lubricated bearings if relatively close axial clearances are maintained.

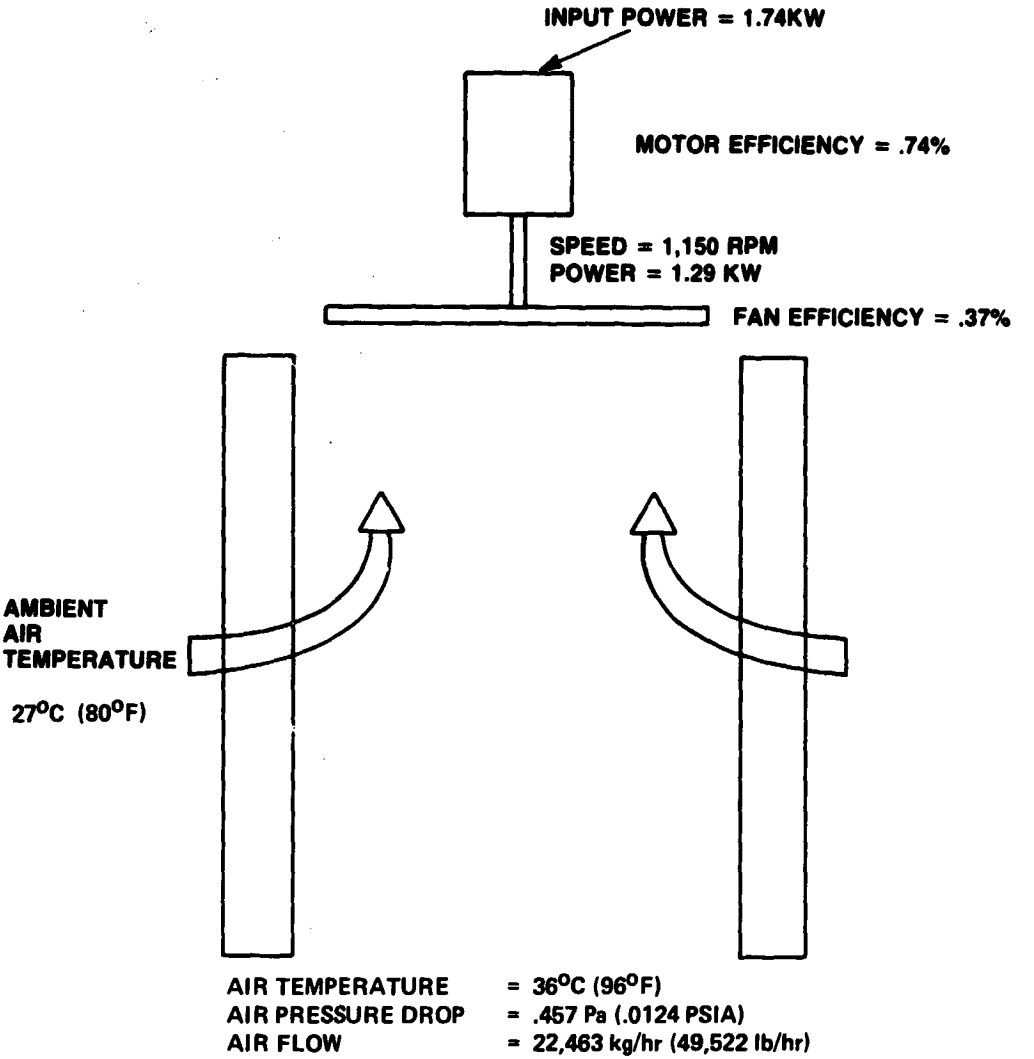

Figure 13 Heat Rejection System

In order to protect the bearing surfaces in the event of a rub, the surfaces would employ a coating. Development of the two stage turbine system would require a materials evaluation in order to select the optimum coating combination. A good first choice would be plasma-sprayed chrome oxide on both surfaces, applied over a softer substrate coating on the turbine wheel to prevent any propagation of cracks from the coating into the Inconel wheel material. Other coatings such as KAMAN SCA or DuPont Triballoy 400 would be likely candidates. Carbon might operate very well for the stationary bearing pads if the operating temperatures were not too high for the binder material.

The operation of the hydrostatic bearing is summarized in Table XII. It should be noted that the thrust-bearing power losses, although relatively large, appear as a heat addition to the turbine. Thermal analysis showed that the heat is distributed approximately equally between first and second stages and hence is partially recovered in the reheater and regenerator.

Table XII Thrust-Bearing Summary

Bearing Outer Diameter	13.7 Cm	(5.4 In)	
Bearing Inner Diameter	10.2 Cm	(4.0 In)	
Bearing Arc Length	9.40 Cm	(3.7 In)	
Supply Pressure	1.40×10^2	KPa	(20 Psia)
Exit Pressure	1.23×10^2	Pa	(1.79 Psia)
Supply Temperature	482°C	(900°F)	

Bearing Eccentricity	Bearing Load Capacity		Bearing Stiffness		Power Loss	Film Thickness		Recess Pressure	
	N	(Lb)	N/m	(Lb/In)	Watts	μm	(In)	Kln	(Psia)
0	0	0	2.89×10^6	16500	359	25.4	.0010	29.0	4.21
.1	7.52	1.69	3.03×10^6	17442	398	22.9	.0009	33.2	4.82
.2	15.8	3.56	3.57×10^6	20360	448	20.3	.0008	38.7	5.62
.3	26.0	5.85	4.59×10^6	26208	512	17.8	.0007	46.5	6.75
.4	39.8	8.95	6.47×10^6	36922	598	15.2	.0006	57.9	8.40
.5	60.2	13.53	9.99×10^6	57037	717	12.7	.0005	75.2	10.9
1.0	133.	30.0	—	—	—	0.	0.	138.	20.0

4.2.5 Radial Bearings

The radial bearings are water lubricated, tilting-pad, journal bearings. The bearings comprise four 80° arc pads, pivoted at 55% of the arc length from the leading edge with a shape designed to minimize inertia about the pivot point. Cool lubricant from the boost pump is injected into the leading edge of each pad where a generous leading edge radius aids in introducing the fluid into the bearing clearance. The bearings, as configured in the conceptual design employ individual pivot pins which are used to preset the bearing clearances in a matched assembly. In mass production the pads would be configured to pivot directly in the housing and a selective assembly procedure used to obtain required clearances. The assembled clearance of 25.4 μm (0.001 inches) is less than the machined clearance to provide additional pad stabilizing forces by virtue of the resulting preload.

Bearing diameters were selected to minimize shaft stiffness. However, the pump-end bearing minimum diameter was limited by the size of the pitot probe. In order to keep bearing losses low, a bearing length-to-diameter ratio of 0.5 was selected with diameters of 1.52 cm (0.6 inches) and 2.08 cm (.82 inches) for the turbine and pump end respectively. The corresponding power losses at design speed are 58 and 145 watts and minimum film thicknesses 8.9 μm (0.00035 inches) and 10.9 μm (0.00043 inches). The bearings are shown in Figure 23. Bearing stiffnesses are plotted in Figure 24 for the two different size bearings and for loading conditions corresponding to vertical and horizontal operation of the system. The bearing stiffnesses were incorporated with the rotor geometry into a critical-speed program. This program is based on the Prohl method and accounts for bearing stiffnesses, shaft lateral and torsional stiffnesses, shaft weights and concentrated weights, polar and radial moments of inertia and their gyroscopic stiffening effects. Figure 25 shows the rotor geometry input into the progam and Figure 26 shows the results of the analysis. Figure 26 shows critical speeds plotted as a function of bearing stiffness and bearing stiffness plotted as a function of speed. The intersection of the appropriate curves shows where critical speeds will occur for varying loads, shown by circles in the figure. In all cases the only critical speeds encountered are rigid body criticals with nodes between the bearings. These generate high damping in the liquid-lubricated bearings and will cause no problems. The third critical speed is a bending critical but occurs well above the operating speed. No critical speeds occur within the operating speed range of the unit.

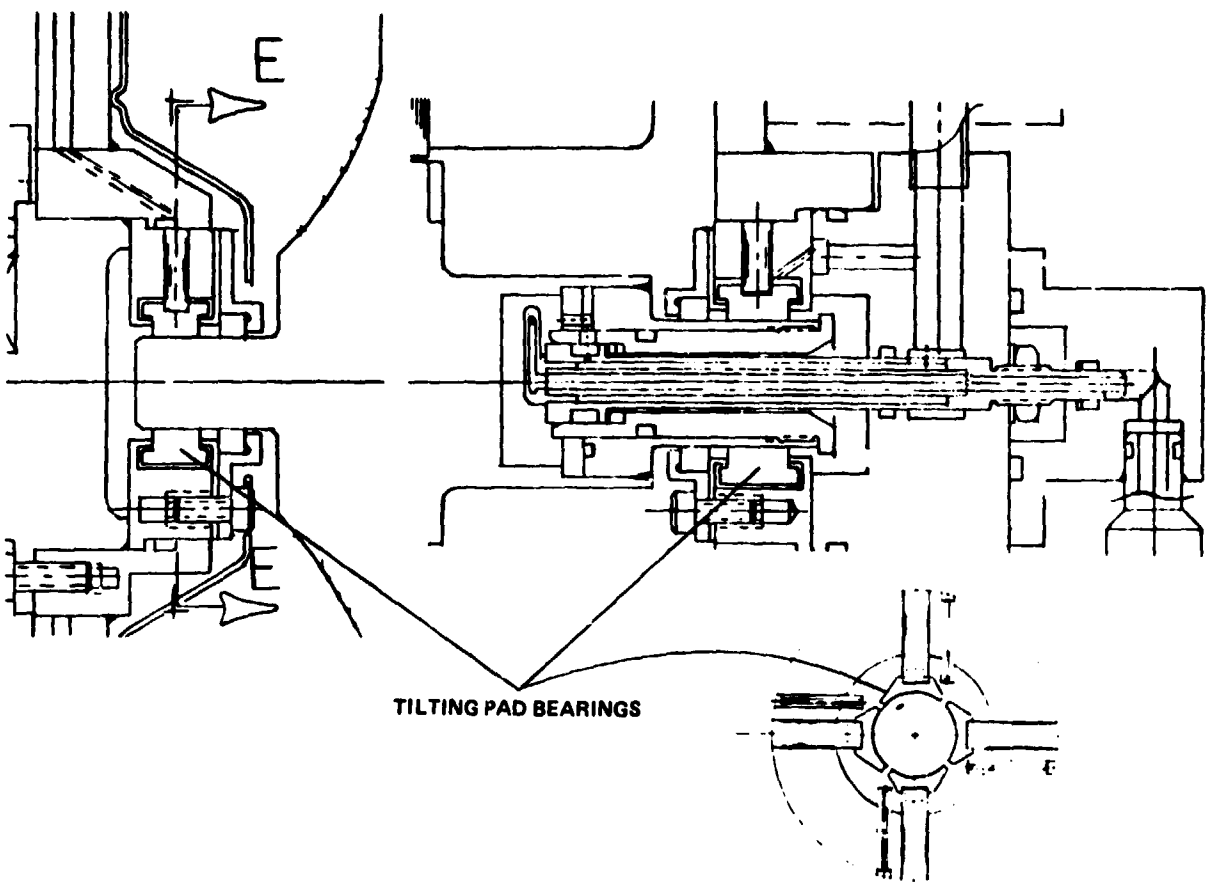

Figure 23 Tilting Pad Bearing Configuration

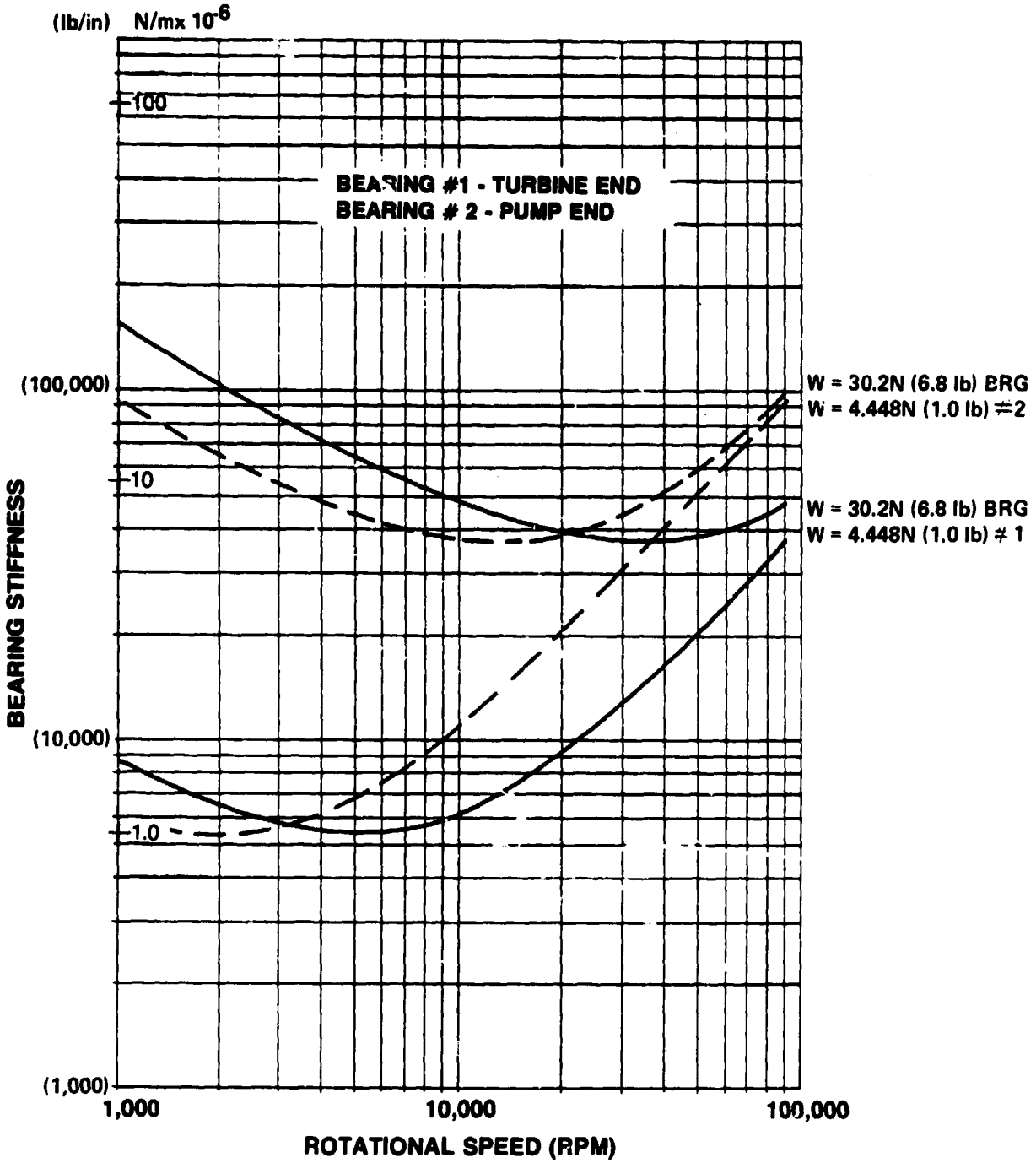

Figure 24 Bearing Stiffness

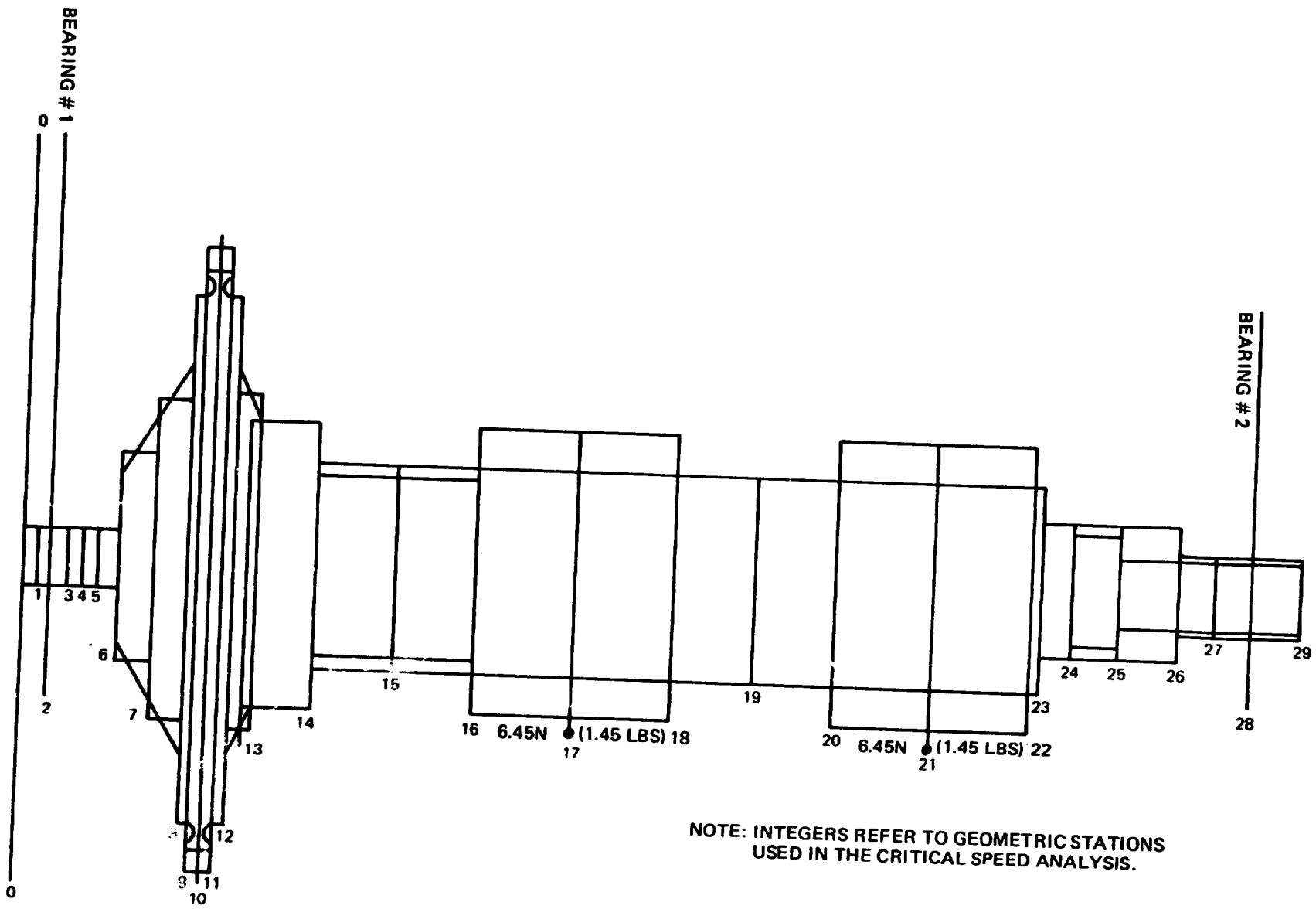

NOTE: INTEGERS REFER TO GEOMETRIC STATIONS USED IN THE CRITICAL SPEED ANALYSIS.

Figure 25 Rotor Geometry

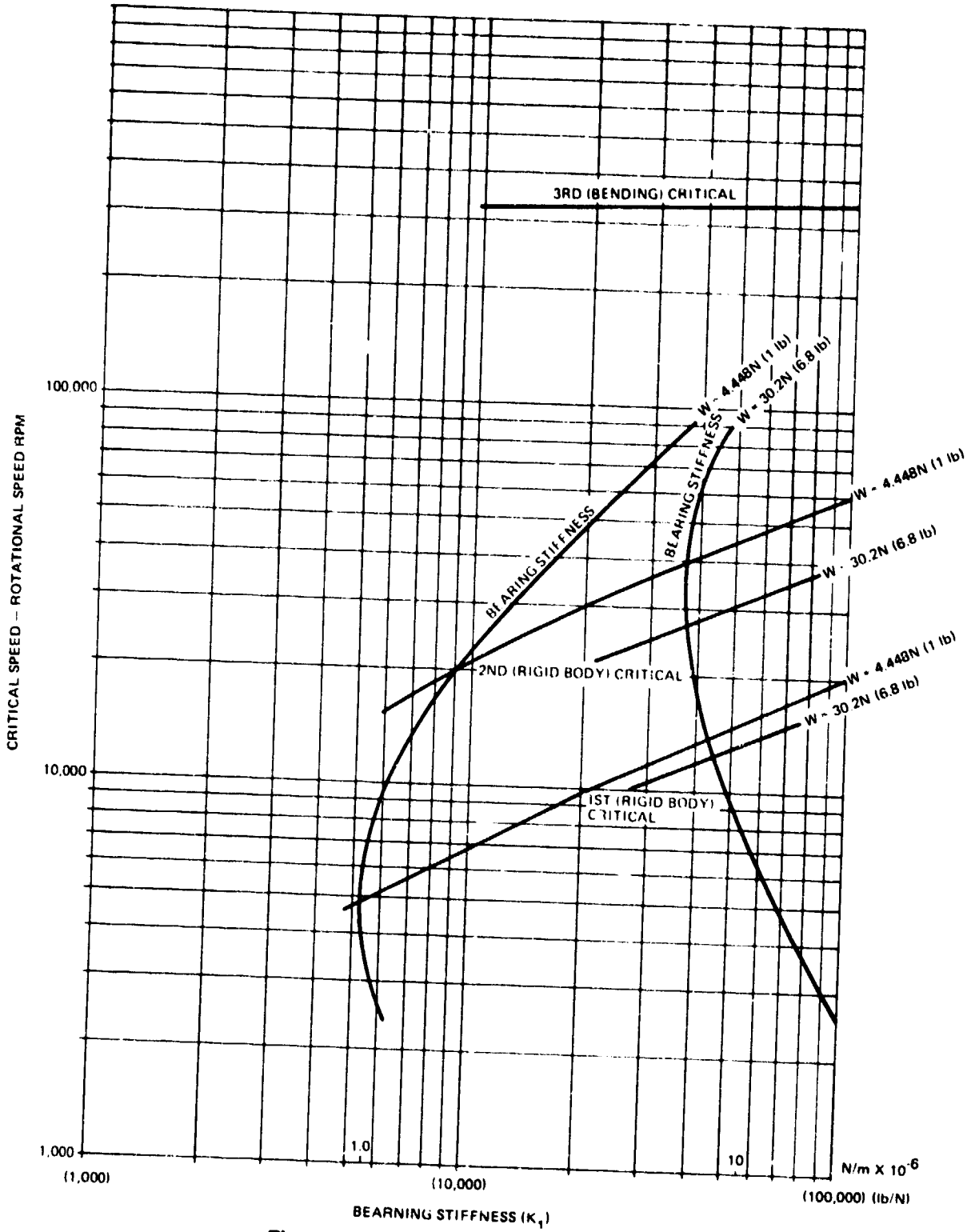

Figure 26 Rotor Critical Speed Map

4.3 PACKAGING AND INTERFACES

The system outline drawing showing overall system dimensions, mounting locations, center of mass and plumbing lines to and from the receiver is presented in Figure 27.

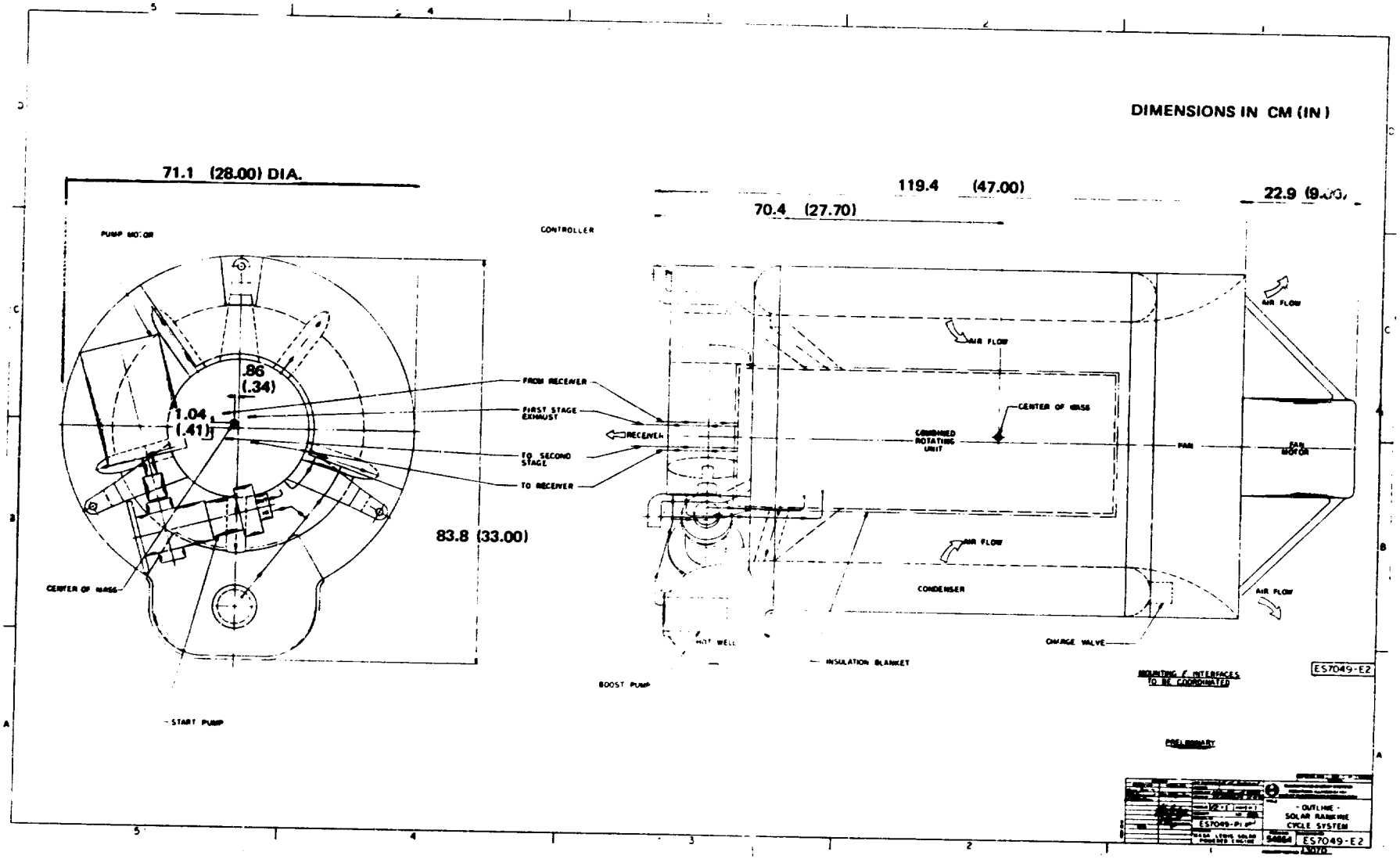

Figure 27 System Outline Drawing

The system has been packaged to minimize collector blockage, although at 71 cm (28 inches) the diameter is greater than desired. Final plumbing and mounting interfaces to the receiver would need to be coordinated. A system weight summary is presented in Table XIII.

Table XIII Weight Summary

COMPONENT	WEIGHT	
	Kg	Lb
Alternator	23.6	52
Turbine Wheel	1.3	2.9
Housings	59.0	130
Regenerator	3.3	7.2
Condenser	43.1	95
Condenser Fan/Motor	39.9	88
Inventory	9.1	20
Valves, Plumbing, Etc.	11.3	25
Auxiliary Pumps	17.2	38
Electronic Controller	9.1	20
Total	217	478

The plumbing connections between the engine and receiver would need expansion compensation, preferably in the form of bellows.

Figure 28 shows the layout drawing of the CRU and regenerator with some of the plumbing, and Figure 29 is a schematic which shows the plumbing arrangement for the CRU-regenerator, with demountable fittings delineated.

Careful consideration has been paid to the design of the CRU-regenerator package to minimize thermal interactions and potential leakage areas both inboard and overboard. For a subatmospheric condenser pressure, air inleakage would cause poisoning of the condensing surfaces and significant performance degradation as well as leading to materials problems due to the presence of oxygen.

Four plumbing lines pass from the power conversion system (PCS) to the heat receiver, these being liquid into the boiler, steam to the first stage and steam to and from the reheater. It has been assumed that all these lines would be of an all-welded construction with expansion compensation incorporated. Consequently, the bottom plate of the CRU-regenerator housing becomes a permanent part of the receiver. Removal of the PCS is accomplished by dropping the bottom from the regenerator housing allowing access to internal fittings in these four lines and the regenerator liquid inlet line. The CRU-regenerator housings can then be split to give access to the on-off valve and the regenerator. The regenerator housing is a permanent assembly welded to the condenser, but the regenerator heat exchanger can be removed as a separate unit. Removal of the valve and remaining plumbing from the turbine bearing support plate allows this water-cooled plate to be removed along with the bearing module. After removal of the pitot probe support housing the rotating assembly, complete with nozzle blocks, can be removed from the housing. The alternator stator can be removed, if required.

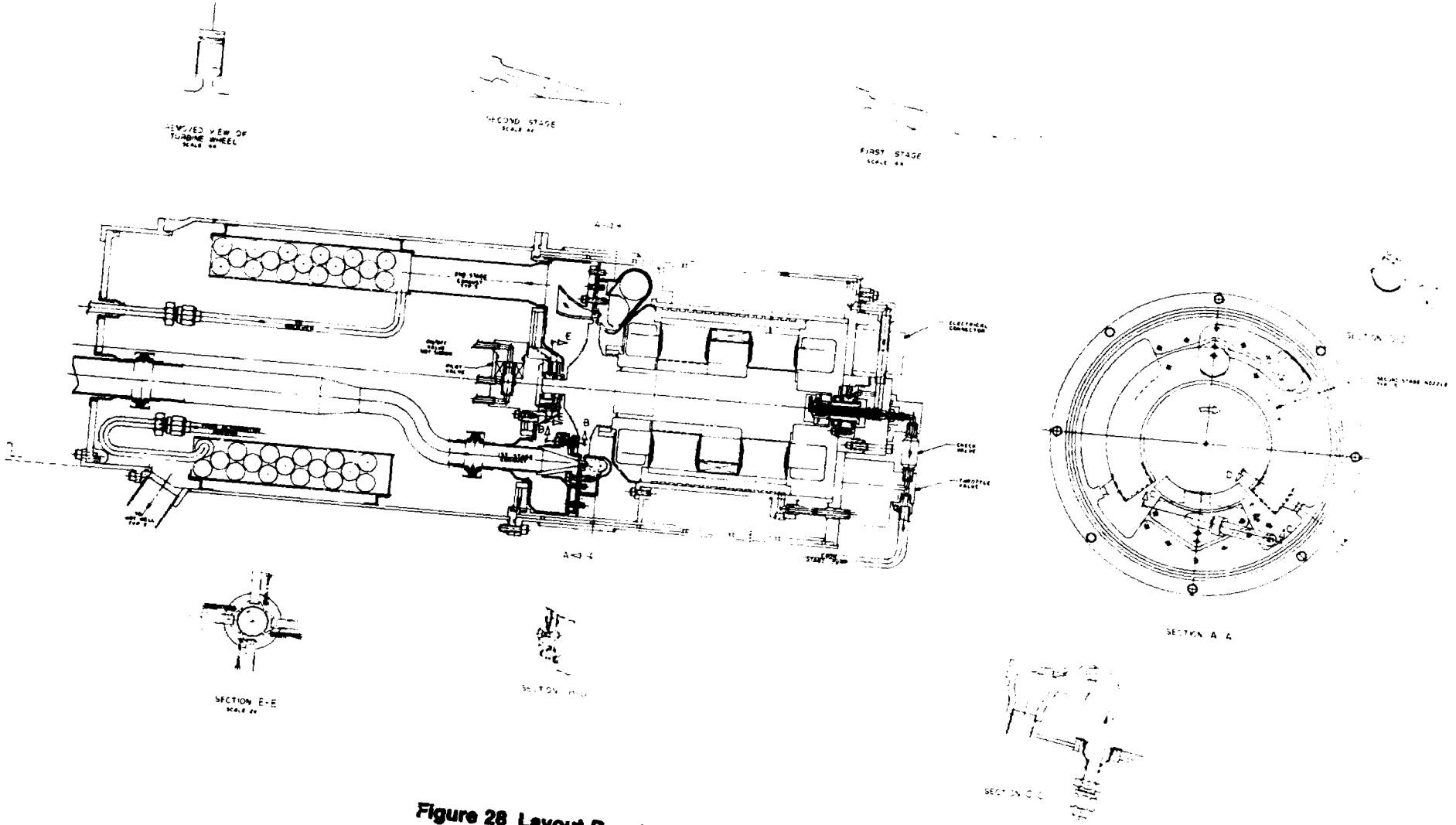

Figure 28 Layout Drawing of CRU-Regenerator

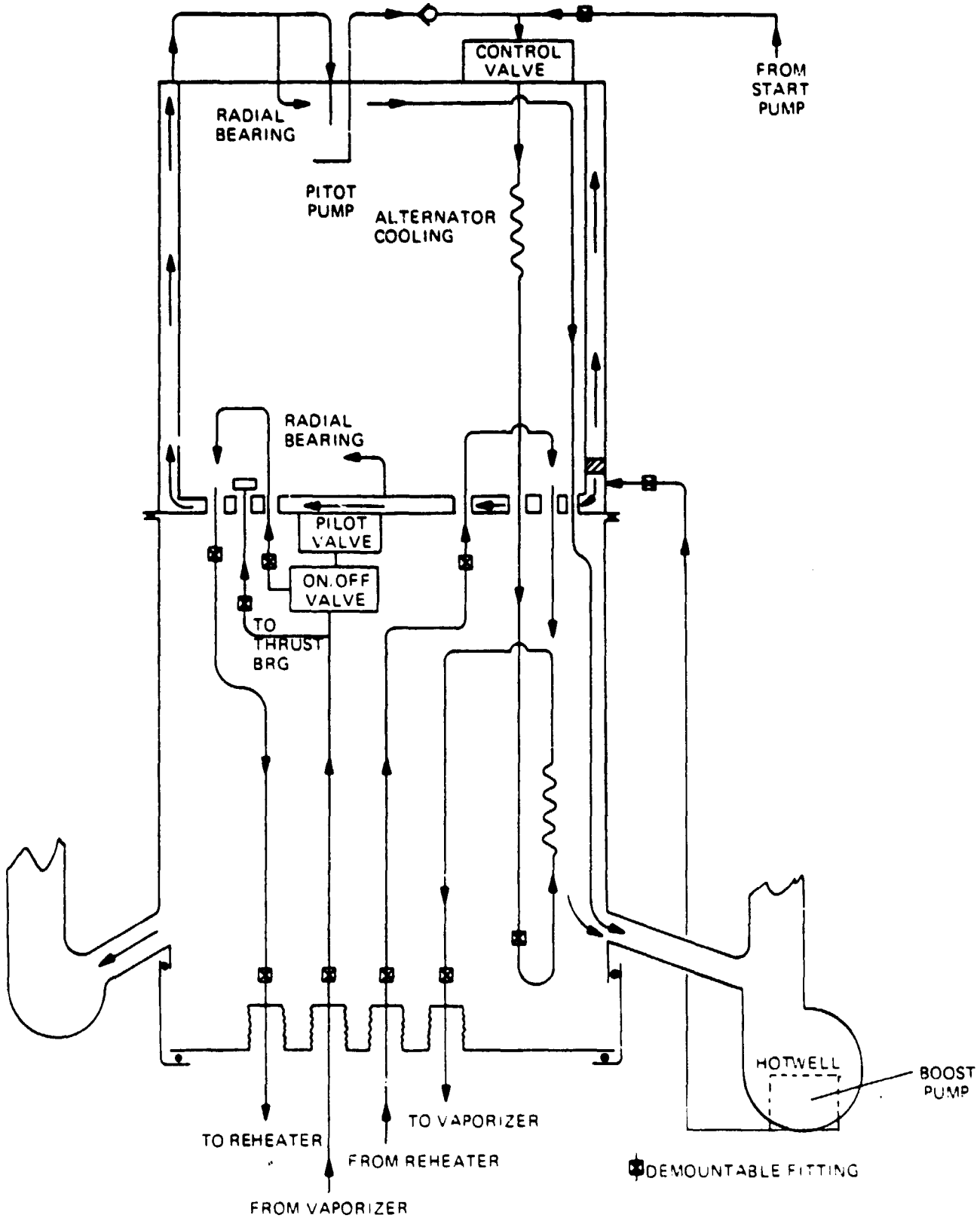

Figure 29 CRU-Regenerator Plumbing Schematic

Cooling water for the turbine housings enters the side of the double-walled housing, passes across the end plate, supplies the turbine bearing, and then flows up the outer wall before passing to the pump inlet and pump bearing. Pump outlet flow passes through the check valve to the flow control valve and then to the alternator and regenerator.

The internal line sizes were selected to give reasonable pressure drops and at the same time ease the problem of packaging in a confined area. The turbine first stage exit passes out through a 2.54 cm (1.0 inch) line to traverse the cold wall, while the second stage inlet is a 3.18 cm (1.25 inches) line. The second stage diffuser, which has an arc of about 240^0, dumps into the cavity before passing through five 3.81 cm (1-1/2 inches) tubes to the regenerator and then through a similar arrangement to the condenser.

All hot lines are thermally isolated from the cold plate with thermal standoffs while sheet metal false walls are used where appropriate to minimize heat transfer. Bearing drains pass from the bearing cavities on the low side of the unit into one of the vapor tubes to the hotwell.

Consideration has been paid to condensation in the bottom of the regenerator housing. During normal operation there is adequate superheat at the regenerator outlet to prevent condensation in this region. Condensation will occur during a cold start, but it is assumed that cold starts will not occur with the unit vertical. If it were found that condensation during startup led to an inventory control problem, a liquid drain line would be added, connecting the housing to the hotwell.

Two additional aspects of system operation have to be considered; firstly, freeze protection when the system is shut down and, secondly, the removal of excess non-condensible gases.

Freezing of the water would cause considerable problems. For instance, if water were trapped in tubing, the tubes could burst, while if trapped in the rotating assembly, startup difficulties would ensue. The system package is designed to allow liquid to drain from the condenser, regenerator and condenser tubes into the hotwell. Water will not drain completely from the CRU, however, so trace heating capabilities are incorporated. An insulation blanket and heating wires are wrapped around the total CRU-regenerator housing in order to keep the system above 0^0C (32^0F). A similar treatment for the hotwell prevents the liquid inventory from freezing.

In order to prevent transfer of liquid from the hotwell to the condenser tubes by reflux action when shut down, and subsequent freezing on the tube walls, it is necessary to incorporate an inert non-condensible gas in the condenser top header. The header is sized to contain all the non-condensible gas at design condenser conditions, but would allow this gas to completely fill the condenser tubes at 0^0C, 610 N/m^2 (32^0F, 0.0885 psia). This feature would allow the condenser to be self-compensating for ambient air temperature, a significant advantage of the reflux condenser. A charge valve is incorporated at the top of the condenser to allow a known amount of non-condensible gas to be added at assembly.

The total system is designed hermetically, with an all-welded construction where possible and some 'O' ring seals to allow disassembly. If the permeability of the 'O' rings is sufficient to allow significant air inleakage, these joints would be replaced with low temperature solder joints. If air inleakage were still a problem, then the non-condensible gas would need to be completely removed on a regular maintenance basis and the system recharged. However, the reflux condenser allows for inleakage of some air without impacting high temperature materials properties, since the air remains well separated from the hotwell fluid. This is in contrast with a through-flow type condenser where the oxygen would tend to recirculate with the working fluid. In

order to determine when maintenance is necessary, some instrumentation would be required. The simplest form would be thermocouples on the condenser tube near the top header to determine the location of the liquid/non-condensible gas interface.

The hotwell is shaped to allow the total system inventory to be contained independent of attitude without liquid entering the condenser tubes and also to keep the boost pump inlet submerged at all times.

The regenerator comprises alternating rows of double and single coils of finned tubing, arranged in an overall counterflow manner, with the water on the inside and steam passing over the outside. The regenerator is shown in the drawing as an annulus in which each circular tube is brazed or welded to the adjacent tube. This, however, is an expensive process and alternate methods could be employed in mass production, for instance a 'C' shaped heat exchanger matching the turbine exhaust arc with each tube joined together with a 'U' bend in a furnace-braze operation. Alternatively the complete heat exchanger could be wound from a single tube. Material considerations led to the selection of stainless steel for both fin and tube, requiring a brazed-fin construction. Copper alloys are used in steam environments, but the corrosion rates are probably too high for a 30-year life.

The condenser has an overall annular shape with the finned tube heat exchanger tubes running the length of the cylinder, forming parallel tubes. The air flows across the finned tube from outside to inside. Ambient air for heat rejection allows the use of aluminum fins formed over a stainless steel tube. This reduces both weight and cost. The tubes would be furnace-brazed into the stainless steel headers.

A summary of regenerator and condenser geometries is given in Table XIV.

Table XIV Heat Exchanger Summary

		Condenser	Regenerator
Tube Material		Stainless Steel	Stainless Steel
Fin Material		Aluminum	Stainless Steel
Header Material		Stainless Steel	—
Tube Diameter	Cm (In)	2.54 (1.0)	.79 (.312)
Fin Outside Diameter	Cm (In)	4.45 (1.75)	1.91 (.75)
Fin Density	Fins/Cm (Fins/In)	3.5 (9)	4.7 (12)
Annulus Outer Diameter	Cm (In)	71.1 (28)	25.4 (10.)
Annulus Inner Diameter	Cm (In)	50.8 (20)	17.5 (6.9)
Annulus Length	Cm (In)	71.1 (28)	18.3 (7.2)
Number of Tubes/Rows		78	17
Total Tube Length	m (In)	55.5 (182)	11.3 (37)

Condenser air flow is provided by an axial flow, 6-bladed propellor fan operating at a design point speed of 1150 rpm driven by a 1.5 kw (2 HP) electric motor. The motor has multiple windings to provide three speeds for part power operation. Fan speed turn-down could be provided with an inverter control but this is a much more expensive process. A rubber skirt is provided around the base of the power conversion system to prevent air flow bypassing the condenser.

The power conversion system would be mounted via a three-point-mount to the receiver, while the condenser is supported by the five vapor return lines. The fan motor is mounted on struts attached to the condenser upper header.

Table XV presents a summary of materials used in the system. Stainless steel was selected as the basic material because of the long life requirements. It is possible that corrosion resistant carbon steel (nickel-plated) could be used for all support housings and low temperature plumbing with a considerable reduction in cost. With the low oxygen content of the water, rust generation should not be a major problem.

Table XV Materials — Selected Components

COMPONENT	MATERIAL
Support Housings	Cres 316 S.S.
Liquid Plumbing	Cres 304L S.S.
Hot Steam Plumbing	Inconel 718
Turbine Nozzle Blocks	Inconel 718
Turbine Exhaust Housings	Cres 310 S.S.
Nozzle Block Spacers	Ceramic
Heat Shields	Cres 310 S.S.
Turbine Wheel	Inconel 718 (Nickel & Chrome Oxide)*
Gas Thrust Bearing	Waspalloy (Chrome Oxide)
Alternator Rotor	AISI 8620 (Nickel)
Radial Bearings	AISI 52100 (Silver)
Bellows	Inconel 718
Pitot Pump	17-4 PH
Electrical Windings	Copper (Polyimide Varnish)
Laminations	Silicon Iron (Nickel)

* Materials in parentheses refer to coatings on the base material.

All alloys will suffer some corrosion, but the growth of protective surface films prevents a continuous corrosion process. Acidity in the water inhibits the growth of the protective layer and hence pure distilled water is not recommended but should be slightly alkaline with a pH in the range of 7.5 to 8.5.

In addition the oxygen content of the water must be maintained at low levels to limit availability for oxidation. The preferred additive for chemical scavenging of water is hydrazine with typical concentrations of about 200 ppm. This chemical is volatile and therefore leaves no residues and in addition provides slight alkalinity. Higher levels of alkalinity are typically obtained by using volatile amines such as morpholine or cychohexylamine. The use of sodium sulphite as an oxygen scavenger is not recommended because the nickel based alloys would corrode rapidly from the formation of hydrogen sulphide (reference 9).

4.4 ANCILLARY EQUIPMENT

Two valves are used in the system. System flow is varied to maintain a constant turbine inlet temperature using a flow control valve. This employs two flapper valves, one of which is driven by a stepper motor whose position is a function of turbine inlet temperature. The other flapper is connected to a bellows to provide pressure compensation. The second valve is an emergency shutdown valve, to be used in the event of a control or alternator failure. Because of the high temperature operation requirements a pilot valve was selected, with two solenoid valves mounted to the cold wall to provide the pilot operation while keeping the solenoid coils cool for long life.

The system start pump is a hermetic, bellows-check valve, positive displacement pump driven by a 0.37 kw (1/2 HP), 900 rpm electric motor.

Electrical conditioning is necessary to convert the high frequency alternator output into the 60 Hz power. The system was designed to be connected into a grid which could absorb all the power generated. The conditioning technique employed is a DC link system employing a line commutated inverter in which the 60 Hz grid provides the switching control for the SCRs. A block diagram is shown in Figure 30. The high frequency power is rectified and then inverted to 60 Hz. The voltage level results in relatively low losses giving a conversion efficiency of 94%.

A system which would have to stand alone to provide remote power would use a different inverter type, such as a pulse width modulated inverter, which would have an efficiency of about 93%.

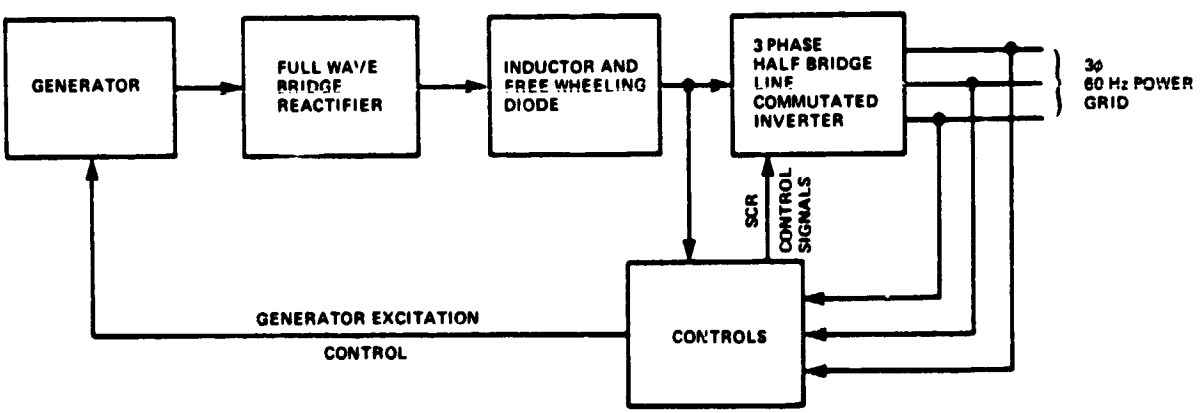

Figure 30 Electrical Conditioning Block Diagram

4.5 SYSTEM CONTROLS

The electrical schematic is shown in Figure 31. The control scheme for parallel operation with the grid assumes that all generated power can be absorbed. This allows the speed to be controlled by varying the alternator field excitation current. The turbine inlet temperature is maintained constant by varying the system flow, thereby matching heat absorbed with available solar energy. As the flow rate drops and power output capability is reduced the output power is lowered by decreasing the field current. As output power decreases, system efficiency is improved by reducing turbine and fan rotational speeds to reduce parasitic losses.

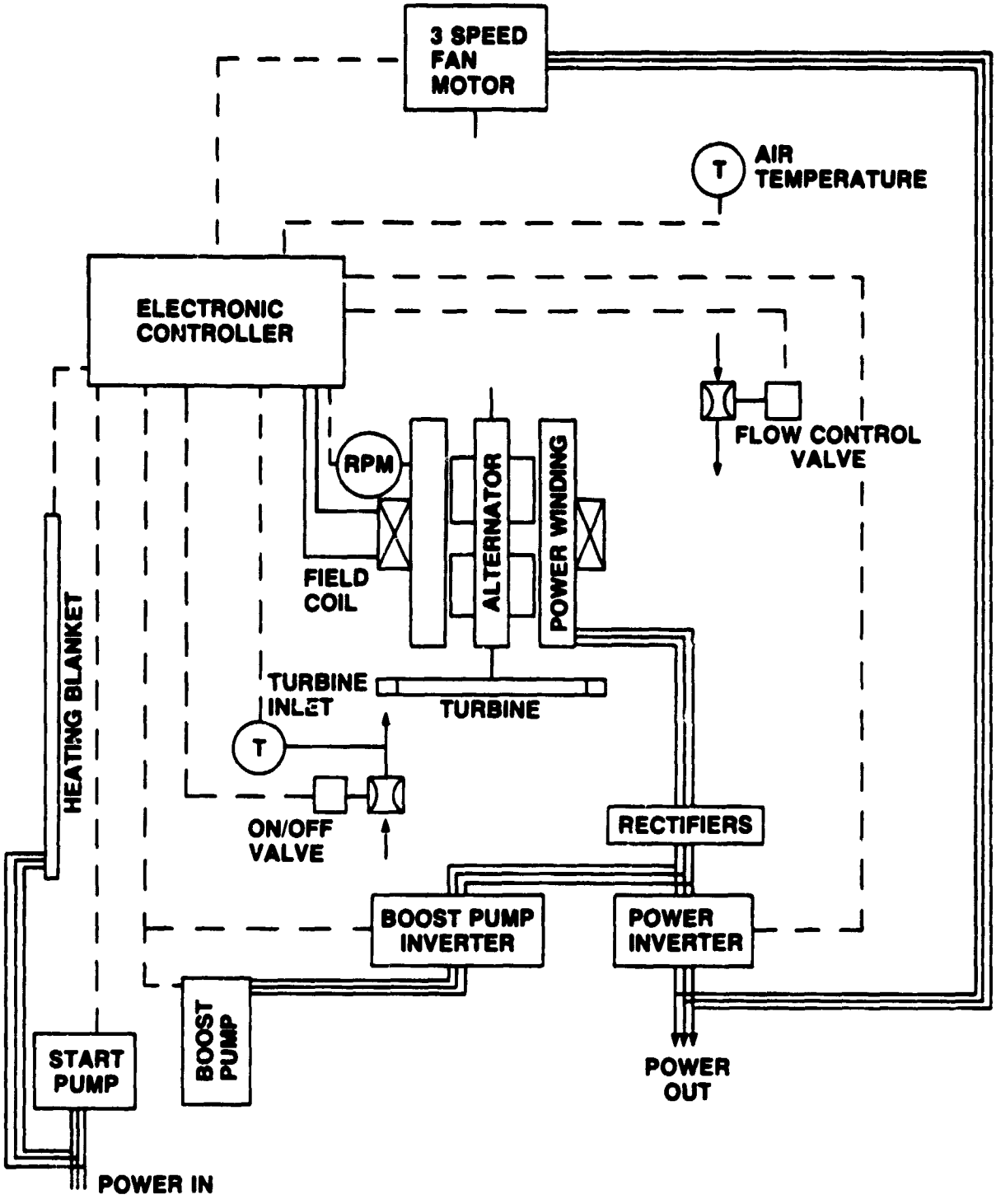

Figure 31 Electrical Schematic

The output power is sensed and used to reduce these speeds per a prescribed turn-down schedule. In addition, the ambient air temperature is sensed so that fan power can be reduced when ambient air temperatures are lower than the design point. All these functions are achieved by using a microprocessor controller to provide the appropriate turn-down schedules as a function of measured parameters. Condenser tube temperatures will also be sensed by the microprocessor to give a warning of excessive non-condensible gas build-up.

A quantitative description of the operation of the system is provided in Figures 32 and 33 by showing the relative changes of major operating parameters. Figure 32 describes steady state operation as a function of thermal input level with the effect of using salt storage on the system also shown. Figure 33 shows startup and shutdown characteristics as a function of time for a system with and without thermal storage. The effect of thermal storage in allowing the system to operate through cloud cover (when the thermal input power drops below a level adequate for self-sustained operation) can be clearly seen. The start mode with and without storage is different. Without storage the start pump is activated just prior to acquiring the sun and then the turbine inlet temperature slowly rises. With storage the thermal energy would be used initially to melt the salt before the system start pump is activated. Salt conditions would be monitored to determine when a fully melted condition was achieved at which point the start pump would be activated. Turbine inlet temperature and output power then rise very rapidly. When the turbine rotational speed reaches the self-sustaining value the start pump is deactivated.

4.6 OFF-DESIGN PERFORMANCE

An off-design computer program was modified to enable prediction of system performance at part power condition. Component off-design performance subroutines were incorporated for the turbine, regenerator, condenser and pump. The orientation of the system was determined as a function of input relative thermal power by assuming vertical orientation at noon and a minimum depression of 15 degrees above the horizontal. Both radial and axial bearing loads vary with orientation and these values were used as input to determine the resultant bearing losses.

Floating visco seals, to separate the bearing cavities from the turbine and alternator cavities, were designed to be of the same size as their respective bearing diameters and to be capable of sealing a pressure differential of 41.4 kpa (6 pounds/in^2). The losses for these seals were added into those of the radial bearings and were calculated as a function of rotational speed.

Initial calculations of off-design performance were implemented with constant fan and CRU rotational speeds using an ambient air temperature of 26.7°C (80°F). Further analyses were then performed at 10.0°C (50°F) and 37.8°C (100°F) ambient air temperatures. The effect of decreasing the fan and CRU rotational speeds was then investigated as a function of thermal power levels and ambient air temperatures. It was found that considerable improvement in system performance could be realized at lower power levels.

At each power level the variation of output power with air flow rate, fan power and CRU rotational speed was investigated and then the operating conditions selected to maximize output.

For this investigation it was assumed that the fan motor would have multiple windings to allow it to operate at three speeds, 100%, 75%, and 50%. This would be achieved by operating with 6, 8, and 12 poles, respectively. The fan performance at reduced speeds was estimated using standard fan similarity laws.

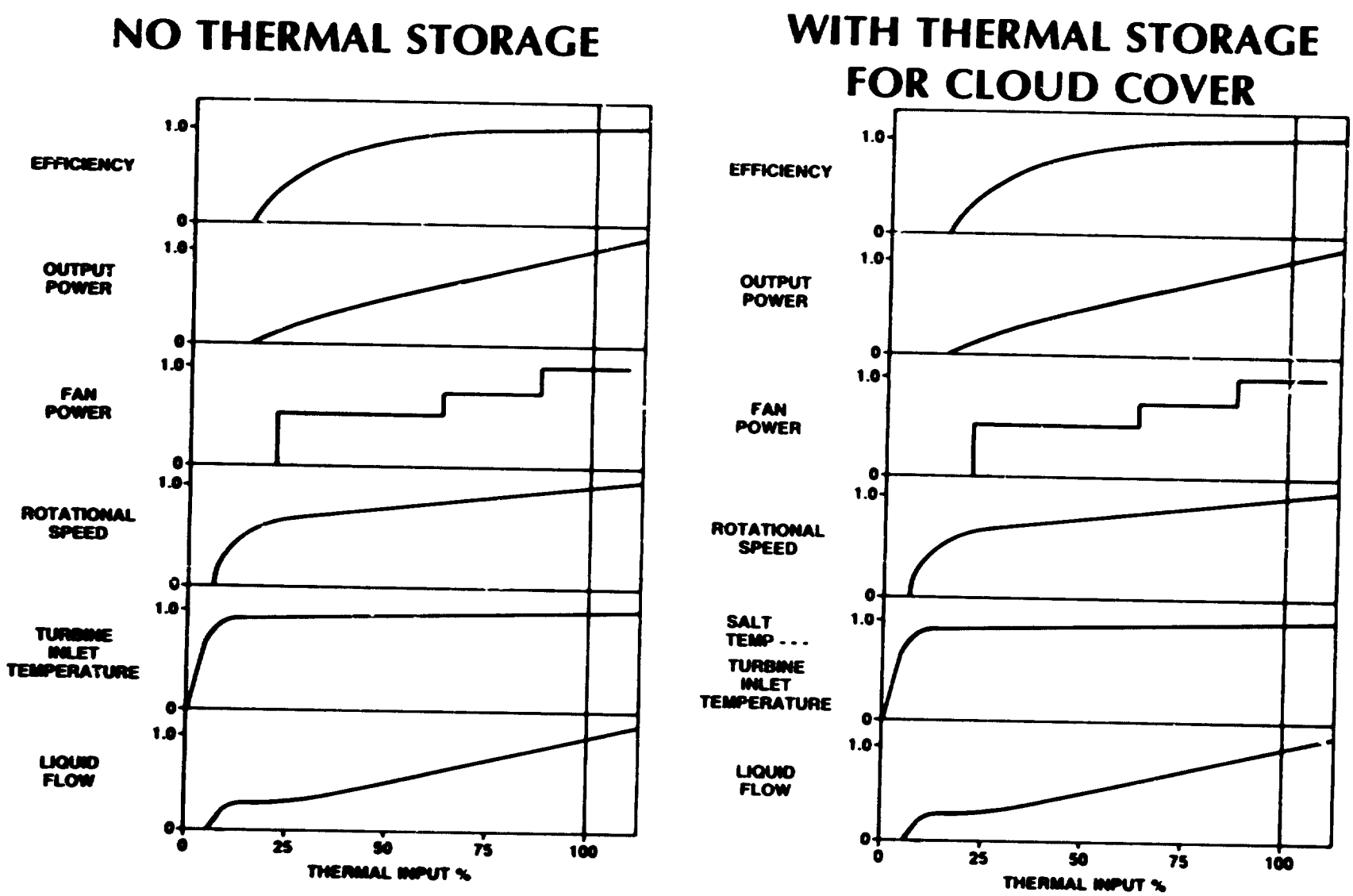

Figure 32 Steady State System Operation

NO THERMAL STORAGE

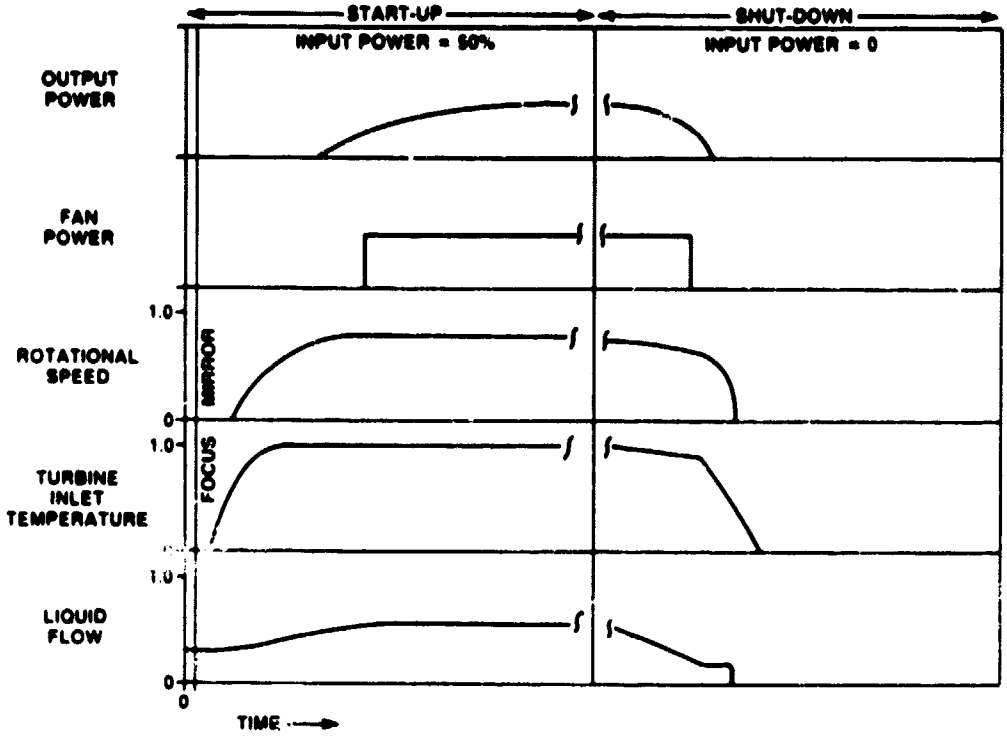

WITH THERMAL STORAGE FOR CLOUD COVER

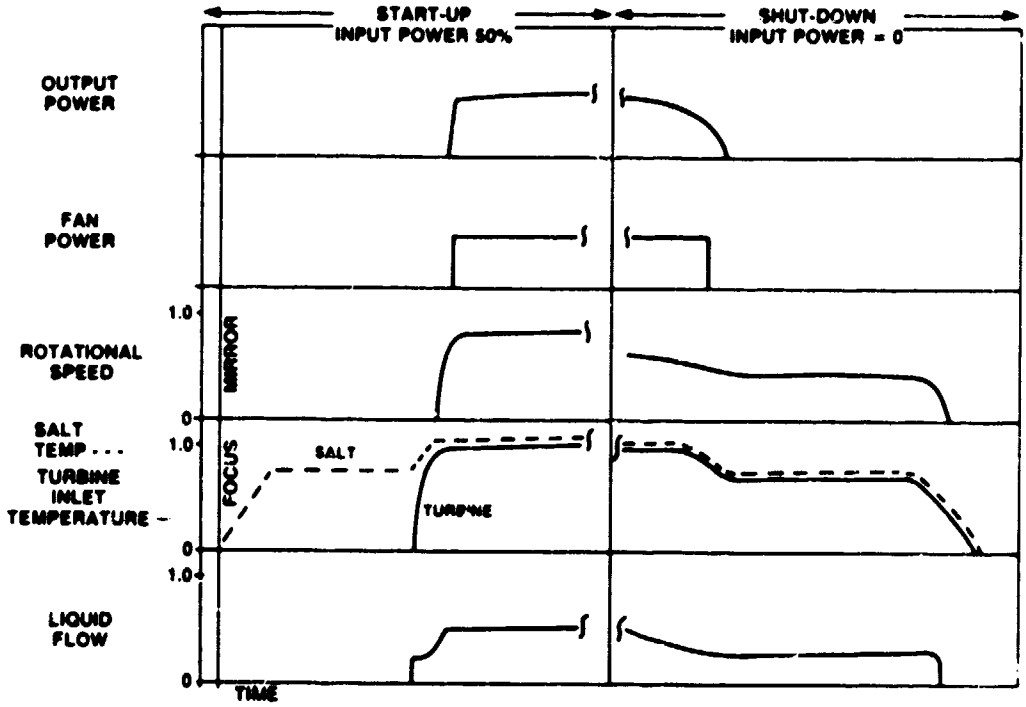

Figure 33 System Transient Operation

It was assumed that the fan motor efficiency dropped from 74% at full speed to 63% at half speed.

In Figure 34 system efficiency and output power is shown plotted as a function of thermal input for 26.7°C (80°F) ambient air temperature. Figure 35 shows the effect of ambient air temperature on system performance with variable fan and CRU speeds.

Table XVI summarizes off-design performance over the nominal annual duty cycle. Based on these data the system will produce 57,052 kw-hours of 60 Hz power annually with a net annual production efficiency of 26.9%. The table shows the step changes in fan power and condenser conditions resulting from varying the fan speed.

The calculation results show that system efficiency drops only by 5% for a 50% reduction in thermal input when the turbine and fan rotational speeds are decreased with output power. If these speeds are maintained constant, a 15% reduction in efficiency results for the same thermal turn-down. In addition, it can be seen from Figure 34 that the system remains self-sustaining down to about 10% thermal input.

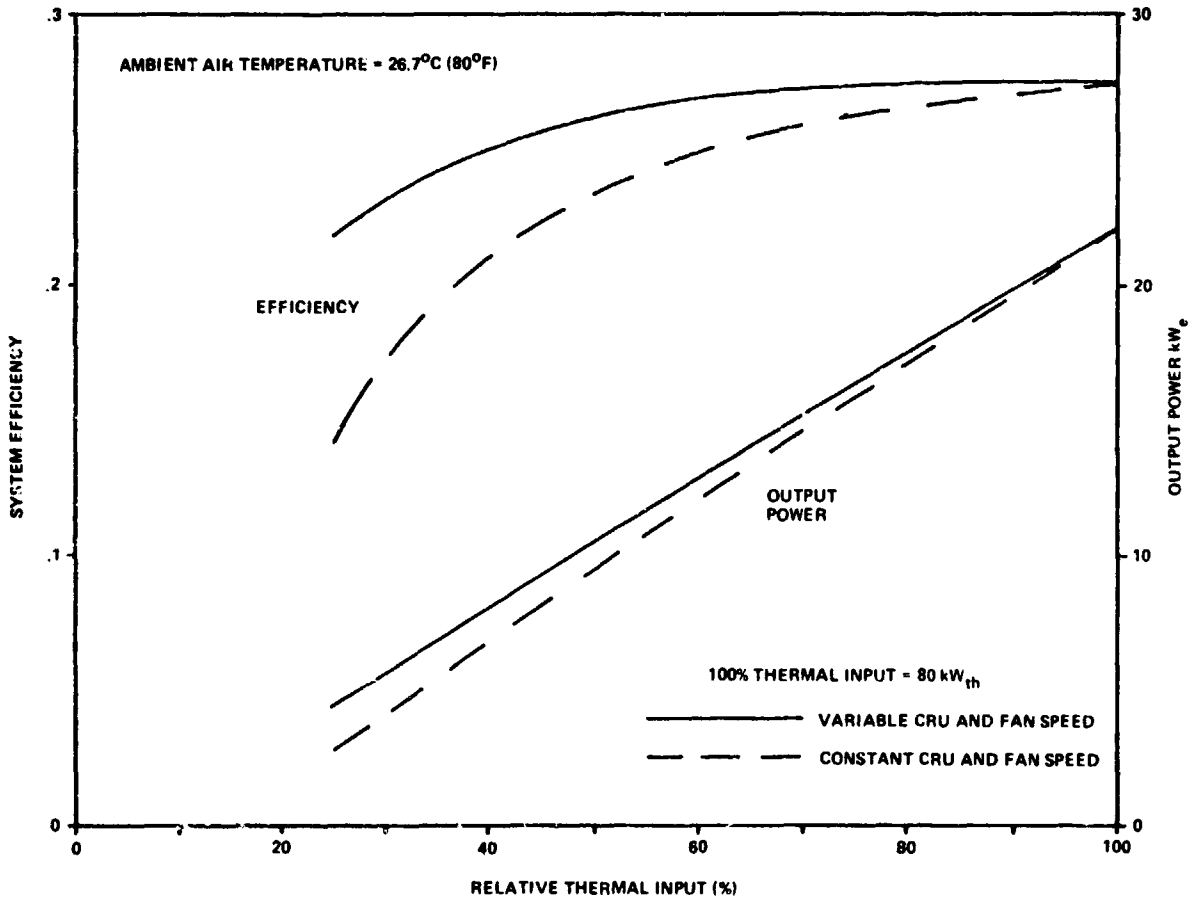

Figure 34 Off Design Performance At 26.7°C (80°F) Ambient Air Temperature

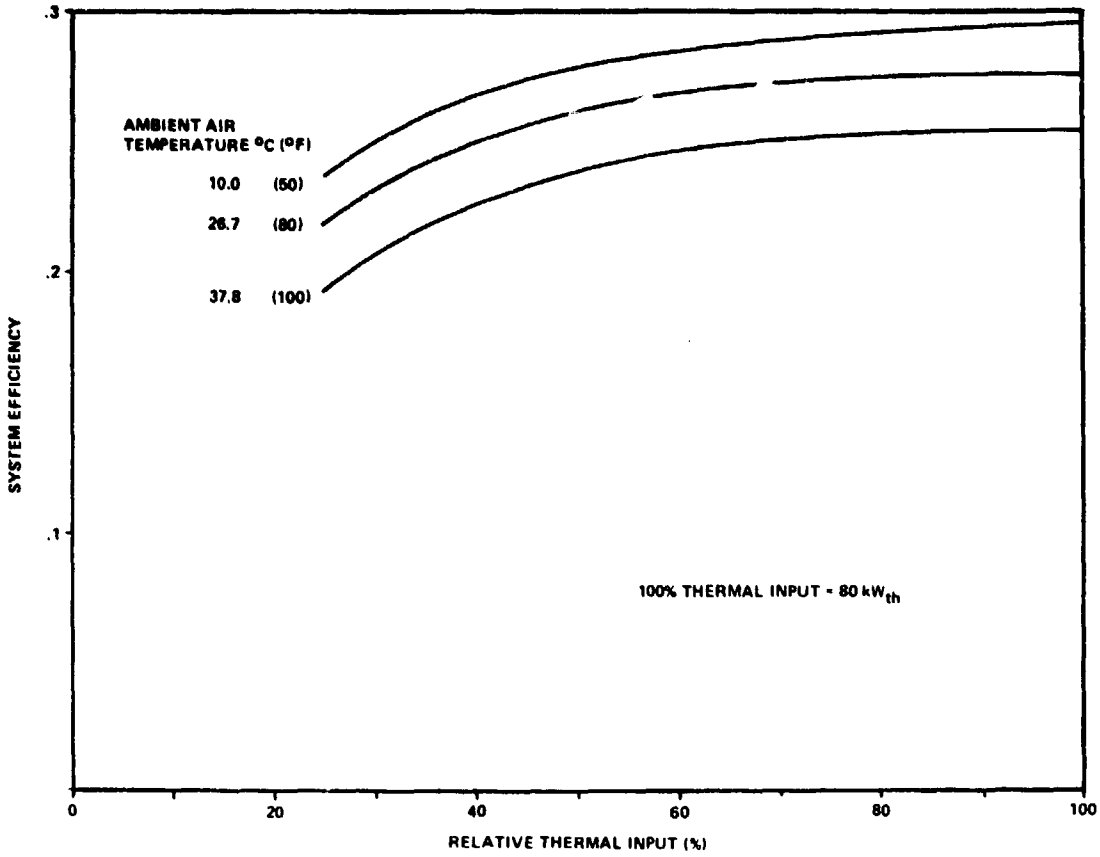

Figure 35 Effect Of Ambient Air Temperature On System Performance

Table XVI Off Design Performance — Nominal Annual Duty Cycle

System Performance

RELATIVE THERMAL INPUT	TURBINE INLET PRESSURE MPa	(PSIA)	TEMPERATURE °C	(°F)	FLOW RATE Kg/Hr	(Lb/Hr)	CONDENSER PRESSURE KPa	(PSIA)	TEMPERATURE °C	(°F)	EFFICIENCIES TURBINE	ALTER-NATOR	ENGINE	AUXILIARY POWER KW$_e$
1 00	4 13	599	732	1350	80 7	178	11 4	1 65	48 7	119	64	937	307	1 84
95	3 92	569	732	1350	76 7	169	10 8	1 57	47 2	117	639	937	305	1 84
92	3 80	551	732	1350	74 4	164	10 5	1 52	46 7	116	638	937	304	1 84
90	3 76	548	732	1350	73 9	163	12 9	1 87	50 6	123	631	937	310	87
86	3 61	524	732	1350	70 8	156	12 1	1 76	49 4	121	629	936	310	87
83	3 48	505	732	1350	68 0	150	11 7	1 69	48 9	120	628	936	310	87
76	3 19	463	732	1350	62 6	138	10 7	1 55	47 2	117	625	936	308	87
65	2 74	398	732	1350	53 5	118	9 17	1 33	43 9	111	617	935	302	87
50	2 17	315	732	1350	42 3	93 2	9 58	1 39	45 0	113	591	930	293	36

Annual Power Production

THERMAL POWER RELATING INPUT	ACTUAL INPUT (kW)	ANNUAL DURATION (HRS)	INPUT kW - HRS	ELECTRICAL POWER OUTPUT kW$_e$	OUTPUT kW$_e$ - HRS	60 Hz AC SYSTEM EFFICIENCY
1 00	80 0	100	8000	21 6	2160	270
95	76 0	400	30400	20 44	8176	269
92	73 6	400	29440	19 72	7888	268
90	72 0	400	28800	19 66	7864	273
86	68 8	400	27520	18 78	7512	273
83	66 4	400	26580	18 13	7252	273
76	60 8	400	24320	16 4e	6592	271
65	52 0	400	10800	13 78	5512	265
50	40 0	400	16000	10 24	4096	256
TOTAL		3300	211840		57052	

5.0 IMPLEMENTATION ASSESSMENT

The manufacturing implementation assessment was based on the final system conceptual design.

5.1 TECHNOLOGY STATUS

Individual components in the system were studied and an estimate made of the type of development required to bring the component to operating status.

Table XVII shows estimates of development times and costs. Many components are considered to be state-of-the-art and therefore would require no development. The component needing most development would be the gas thrust bearing. A large proportion of this development time would be a material screening effort.

It should be noted that the drawings shown represent a development-type unit rather than a mass-produced unit.

Table XVII Component Status

Component	Similar System Application	Development Time (Months)	Development Cost (78 Dollars)
Start Pump	Purchased	—	
Boost Pump	ORC*	—	
Boiler Feed Pump	ORC	6	40,000
Flow Control Valve	ORC	—	
On/Off - Relief Valve	—	12	100,000
Condenser	ORC		
Regenerator	ORC		
Re-Entry Turbine	Space Shuttle APU	24	600,000
Gas Thrust Bearing	—	24	1,000,000
Homopolar Alternator	ORC	—	
Radial Bearings	ORC	—	
Condenser Fan	Purchased	—	
Fan Motor	Purchased	—	
Controller	ORC	6	50,000

*ORC — Similar components have ben developed in the past for organic Rankine cycle systems.

5.2 PRODUCIBILITY

A parts list was generated for the system and a manufacturing assessment made of the costs of production. For mass production, assumptions were made of ways in which the system could be made cheaper by using castings in place of machined housings and stampings in place of welded sheet metal assemblies. From a parts list and the drawings, set-up and machining times for manufactured parts were estimated and price estimates obtained from vendors for purchased parts.

Table XVIII shows the resulting cost estimates for different annual production rates with a breakdown by major component. These prices represent unit manufacturing cost in 1978 dollars without profit or capital investment such as tooling or production facilities, and do not include amortized cost for preproduction prototype systems.

Table XVIII Component and System Cost Estimates

	NUMBER OF UNITS PRODUCED/YEAR			
	100	1,000	10,000	100,000
TOTAL COST FOR SYSTEM (1978 DOLLARS)	35,000	30,000	15,000	8,000
COMPONENT COSTS (1978 DOLLARS):				
CONDENSER ASSEMBLY	3,400			
CONTROLLER	1,000			
POWER CONVERSION SYSTEM	22,000			
MISCELLANEOUS	3,300			
SYSTEM ASSEMBLY AND TEST	5,300			

The assembly and test costs for a system of this design are high due to the complexity of the two-stage turbine design. The assumptions made for cost reduction as a function of production rate were that 100 and 1000 units per year would be produced in existing facilities, with improved tooling at the high rate. At 10,000 and 100,000 units per year, a dedicated facility would be built with greatly reduced overhead rates. A price break would occur for the higher production rate, mainly due to reduction in material costs. At the highest production rate, the specific cost is 364 dollars/kw.

5.3 DURABILITY

Component 'Mean Time Between Failure' (MTBF) estimates were made based on handbook values, past experience and other system studies. These were applied along with component costs to determine component replacement costs. Labor costs were also incorporated depending on the extent of disassembly required to replace a part. No data base exists for the hydrostatic gas bearing but high speed air bearings have MTBF values of 50,000 hours or better and this information was used for the analysis. This failure rate is an order of magnitude higher than other components of the CRU. All failure rates are mature, i.e., based on developed components.

Maintenance requirements for the system are minimal. The condenser will need cleaning at certain intervals, due to the collection of dust. However, this cleaning can be done when the solar collector is cleaned. In addition, non-condensibles that collect in the condenser due to air inleakage will need to be removed. The frequency depends on the quality control applied to the leak-checking and sealing of the system, which affects system cost. For this study purpose both cleaning and bleeding of the condenser is assumed to be on a monthly maintenance schedule.

The bearings in the valve stepper motor, the fan motor and the start motor would be lubricated once each year, and the bearings of the boost pump replaced after 15 years.

The resulting frequency and costs itemized by major component are shown in Table XIX. The total operation and maintenance cost is $443.61 per annum which reduces to $0.0078/kw-hr.

Table XIX Operation and Maintenance Costs

COMPONENT	MATURE FAILURE RATE PER 10^6 HOURS	REPLACEMENT COST PER YEAR	SCHEDULE MAINTENANCE	MAINTENANCE COST PER YEAR
COMBINED ROTATING UNIT	25.3	101.07		
TURBINE	(.1)			
ALTERNATOR	(.2)			
FEED PUMP	(.4)			
RADIAL BEARINGS	(2.3)			
SEALS	(2.3)			
GAS BEARING	(2.0)			
HEAT EXCHANGERS (INCLUDING FAN)	4.3	23.61	CLEAN AND BLEED CONDENSER, GREASE FAN MOTOR BEARINGS	175.00
CONTROLLER	35	49.00		
EQUIPMENT	12.5	49.93	GREASE MOTOR BEARINGS	45.00
TOTAL SYSTEM	77.1	223.61		220.00

TOTAL OPERATING COST	$443.61 PER YEAR
DESIGN LIFE	30 YEARS
TOTAL POWER PRODUCTION	57,000 KW-HRS
SPECIFIC OPERATING COST	$0.0078/KW-HR

6.0 CONCLUSIONS

This report covers a feasibility study performed on a solar-powered steam Rankine cycle to generate electrical power using a turbine as the prime mover. Parametric analyses were performed on single and two-stage turbines resulting in the selection of a two stage re-entry turbine for the conceptual design.

It was found that with appropriate selection of materials the steam system could be operated at 732°C (1350°F). Relatively high system efficiencies were achievable with a re-entry turbine configuration but special turbine interstage sealing techniques were necessary to achieve this efficiency.

The sealing concept employed requires advancing the state-of-the-art in gas thrust bearings.

At the system design point of 80 kw thermal input a system efficiency of 27% was obtained based on 60 Hz electrical power output divided by absorbed thermal power. Off-design analyses showed that if turbine and fan rotational speeds were reduced with output power, system efficiency remained very high for significant turndown, reducing by only 5% for a 50% turndown while a 15% reduction occurred if turbine and fan speeds remained constant.

The need for a gas thrust bearing to allow operation of the turbine at close axial clearances led to high system manufacturing and assembly costs and also impacted system failure rates. At mass production rates of 100,000 units per year, a total manufacturing cost of approximately $364/kw was estimated, while operating costs were approximately $0.0078/kw-hr.

7.0 REFERENCES

1. Solar Thermal Power Systems Point-Focusing Distributed Receiver (PFDR) Technology: A Project Description. J. W. Lucas and J. Roschke AIAA/ASERC Conference on Solar Energy: Technology Status. Nov. 1978

2. 15 KWe (Nominal) Solar Thermal - Electric Power Conversion Conceptual Design Study - Steam Rankine Reheat Reciprocator System, Foster-Miller Associates, Inc., H. Fuller, NASA CR-159590, June 1979

3. 15 KWe (Nominal) Solar Thermal - Electric Power Conversion Conceptual Design Study - Steam Rankine Reciprocator System, J. Carter Enterprises, W. Wingenbach, NASA CR-159591, June 1979

4. 15 KWe (Nominal) Solar Thermal - Electric Power Conversion Conceptual Design Study - Brayton Systems, AiResearch Mfg. Co., T. Ashe, NASA CR-159592, June 1979

5. 15 KWe (Nominal) Solar Thermal - Electric Power Conversion Conceptual Design Study - Free Piston Stirling System, Mechanical Technology, Inc., G. Dohat, NASA CR-159587, June 1979

6. 15 KWe (Nominal) Solar Thermal - Electric Power Conversion Conceptual Design Study - Kinematic Stirling System, Mechanical Technology, Inc., H. Nelving, NASA CR-159588, June 1979

7. Compact Heat Exchangers. Kays & London, McGraw-Hill 1964

8. Sealing Behaviour of Superheater Tube Alloys in ASME High Temperature Steam Research Tests at 1100 - 1500^{0}F. F. Eberle and C. H. Anderson, ASME 61-PWR - 3

9. Corrosion, Volume I Edited by L. L. Shreir. John Wiley and Sons.

PAGE 62 INTENTIONALLY BLANK